


Università degli Studi di Cagliari

DOTTORATO DI RICERCA

Scienze e Tecnologie Chimiche

Ciclo XXVI

TITOLO TESI

Stability of dental alloys in artificial saliva: an electrochemical and XPS investigation

Settore/i scientifico disciplinari di afferenza

Chim/01

Presentata da:	Manuela Pisu
Coordinatore Dottorato	Prof. Mariano Casu
Relatori:	Prof.ssa Antonella Rossi – Prof. Bernhard Elsener

Esame finale anno accademico 2012 – 2013

Contents

Abstract

Alloys used in dentistry should have good mechanical properties and a very high corrosion resistance in order to be considered biocompatible. The oral cavity is a potentially highly corrosive environment thus stainless steels have been used frequently. Due to allergic reactions of about 10% of the population to nickel ions new nickel-free stainless steels have been developed. In this PhD thesis the Ni-free stainless steel DIN 1.4456 has been studied with electrochemical and XPS surface analytical techniques at 25°C and at 37°C. Surface analysis has shown that the alloy in artificial saliva forms a protective passive film at both temperatures. At 25°C the oxy-hydroxide film formed is enriched in oxidized chromium, after long immersion times (7 days) the nominal composition of oxidized manganese (18%) is found. Molybdenum in the film is slightly enriched. Angular resolved XPS performed on samples exposed at 37°C clearly indicate that the outer part of the passive film is composed essentially of iron oxy-hydroxide whereas chromium oxy-hydroxide is located at the inner part. Experiments with argon ion sputtering confirm that the inner part of the film is enriched in oxidized chromium and manganese whereas oxidized iron is strongly depleted. Both angle-resolved XPS and experiments with argon ion sputtering show that the alloy beneath the passive film is depleted in manganese.

The kinetics of initial dissolution and film formation are more rapid at 37°C compared to 25°C but seem to follow the same mechanism. At 37°C the initial corrosion rate is much higher but its decrease with time is more rapid. After 24 h the dissolution rate is already lower then 0.2 µm/year, the steady state dissolution rate will be at least one decade lower. This very low dissolution rate has been confirmed by ICP solution analysis where the metal ion concentration was found to be below the detection limit of the technique for all the alloy elements.

Finally a model is proposed that might explain the surface films formed after exposure to artificial saliva solution. During the short initial period with a relatively high corrosion rate iron and especially manganese (non-noble elements) dissolve. Chromium is the film-forming element and an inner chromium oxy-hydroxide film is formed. This film limits progressively the dissolution of the alloy: with time an outer iron oxy-hydroxide film is formed. Due to the dissolution of manganese, the manganese content immediately below the film is strongly depleted. On the contrary, molybdenum is present with about 7%. Such a layered structure

of the surface is responsible for the high corrosion resistance and biocompatibility of the DIN 1.4456 stainless steel.

Riassunto

Le leghe utilizzate in odontoiatria devono essere biocompatibili e oltre che possedere buone proprietà meccaniche, devono avere anche un'ottima resistenza alla corrosione. I fluidi biologici presenti nel cavo orale sono potenzialmente corrosivi e una categoria di materiali utilizzati in ambito dentistico sono gli acciai inossidabili perché possiedono questi requisiti e hanno costi accessibili. La normativa europea ha anche fornito indicazioni in merito all'uso di materiali contenenti nichel limitandone l'uso. È noto, infatti, che questo elemento possa causare allergie in soggetti predisposti: si stima che circa il 10% della popolazione sia sensibile a questo elemento. È stato quindi proposto l'uso di acciai senza nichel e nonostante siano già utilizzati per la costruzione di bracket non sono disponibili in letteratura risultati completi sulla caratterizzazione di questi acciai.

Scopo di questa tesi è lo studio della stabilità di un acciaio con 18% di manganese, DIN 1.4456, mediante tecniche elettrochimiche e di analisi di superficie dopo esposizione alla soluzione di saliva artificiale a 25°C e a 37°C e per tempi diversi, fino a sette giorni. La velocità di corrosione a 37°C è inizialmente più alta che a 25°C ma diminuisce molto più rapidamente con il tempo di esposizione. A 37°C dopo 24 ore si registra una velocità di corrosione inferiore a 0.2 μm/anno. Questi dati sono stati confermati anche dall'analisi delle soluzioni che erano state in contatto con i campioni di acciaio mediante la tecnica AES-ICP.

L'analisi XPS (spettroscopia di fotoelettroni a raggi X) ha dimostrato che sulla superficie dell'acciaio si forma uno strato superficiale di ossi-idrossidi, chiamato film passivo, che è poco solubile sia a 25°C sia a 37°C. A 25°C il film passivo è ricco di ossi-idrossidi di cromo e dopo sette giorni la composizione di manganese raggiunge il 18%, cioè quella nominale della lega. Il molibdeno è invece leggermente arricchito rispetto alla composizione media dell'acciaio. Le misure in risoluzione angolare (ARXPS) compiute dopo esposizione a 37°C, evidenziano che il film passivo è composto di uno strato interno costituito da ossi-idrossidi di cromo e di uno strato esterno costituito da ossi-idrossidi di ferro. I dati ottenuti utilizzando l'abrasione ionica con ioni argon per ottenere il profilo di composizione confermano che la struttura del film passivo è multistrato anche a 25°C. Lo strato interno è costituito da ossi-

idrossidi di cromo e manganese. Tutti gli esperimenti indicano anche che la composizione della lega all'interfaccia bulk-film passivo è depauperata di manganese.

I risultati ottenuti possono essere interpretati ipotizzando che subito dopo l'immersione si abbia un'alta velocità di dissoluzione del ferro e soprattutto del manganese (elementi non nobili) con formazione del film passivo multistrato. È la formazione di questo film protettivo che favorisce la diminuzione della velocità di dissoluzione degli elementi presenti nella lega e porta a un conseguente arricchimento di ossi-idrossidi di ferro nello strato esterno del film stesso. La composizione all'interfaccia film passivo-bulk è impoverita di manganese ed arricchita di molibdeno (circa 7%) a causa della reazione di dissoluzione iniziale della lega. La struttura a strati rende l'acciaio DIN 1.4456 particolarmente stabile e biocompatibile.

1 Introduction

Dental alloy are materials used in dentistry for crown, bridges, prostheses, and implants. They should exhibit good mechanical properties in order to be reliable during handling and loading into the mouth. The difficult loading conditions, which depend on the force of muscles and on the age of the patient, have to be considered as well. Furthermore, dental materials are in contact with environmental conditions in the mouth that might initiate corrosion reactions. The temperature can vary between 5 and 55°C and the composition and the pH of the saliva varies depending on the nutrition [1]. Human saliva is a saline solution, which also contains organic compounds such as proteins. The corrosion reaction consists in the release of metal ions with deterioration of the mechanical properties and potentially toxic effects on the human body. This reaction may also be mediated by the presence of microorganisms [2,3]. The primary purpose in dentistry is to improve the quality of life of the patients. To achieve this, in some cases is necessary, however, to replace or to alter the structure of the tooth. In this case, the main objective is the selection of biocompatible and corrosion resistant materials. Biocompatibility is a fundamental requirement. [4]. The choice of the material for dental applications is very important since there are a wide variety of materials with a different composition and different properties available on the market.

A widely accepted definition of biocompatibility is "the ability of a material to elicit a biological response appropriate in a given application" i.e. a biological response of the material itself and also the ability of the material to resist degradation or corrosion. Biocompatibility of a material and its corrosion resistance in the intraoral environment depends on the patient's condition, the properties of the material and the context in which the material is being used. Since corrosion is a reaction that starts at the surface and it is due to the interaction between the material and the surrounding environment such as the body fluids, a very useful analytical strategy for assessing the material biocompatibility is based on the use of surface analytical techniques. They allow the correlation between the electrochemical measurements carried out in solution with the composition of the surface thus contributing to establish the biocompatibility of the material as it has been demonstrated by many authors [2, 5-9]. *Stainless steels* are used in dental applications especially because they exhibit good mechanical properties at relatively low costs. They are easy to process and have a good corrosion resistance. Nickel bearing stainless steels are presumed to be carcinogenic and might cause allergies and dermatitis. Nickel-free austenitic stainless steels have been studied as valid alternative material to be used in dental applications.

1.1 Aim of the thesis

Stainless steels are used in orthodontics for the production of orthodontic brackets. These materials form an oxide film (passive film) at the surface that protects them from corrosion. The aims of this work is to gain a better understanding of the passive film formation and stability of a nickel-free steel DIN 1.4456 in contact with artificial saliva by means of electrochemical and surface analytical techniques. This should allow a first assessment of the biocompatibility of this new material.

Biocompatibility of a material is a very complex parameter; a final judgment however requires in vitro and in vivo biological tests. Such in vivo tests were not performed in this thesis; results of biological tests obtained by other authors are presented in section 1.7 of this chapter.

Experimental approach

To reproduce the oral environment experiments were performed using "Tani-Zucchi modified" artificial saliva [10] as a model solution at body temperature of 37°C. Electrochemical measurements were carried out for increasing exposure times: 1 hour, 3 hour, 16 hours and 24 hours in order to investigate the effect of exposure duration on the composition of the surface film and on its corrosion resistance. During the immersion tests the open circuit potential (OCP) was recorded, at the end of exposure linear polarization resistance (Rp) was measured in order to determine the corrosion rate. The surface of the DIN 1.4456 stainless steel was characterized qualitatively (oxidation state) and quantitatively (thickness and composition of the passive film and the metal beneath) by XPS surface analysis after different times of immersion into artificial saliva.

Structure of the thesis

The thesis is structured as follows: Chapter 1 presents the introduction and the state of the art on orthodontic materials. Special attention is dedicated to nickel-free stainless steels and to the analytical approaches used for investigating the stability of orthodontic materials. Chapter 2 gives a description of the experimental protocols adopted and the materials used for the research. Chapter 3 reports the results obtained with the electrochemical and surface analytical techniques at various exposure times and at two different temperatures. In Chapter 4 the results of the corrosion tests are compared; in the second part the effect of exposure time and of temperature are discussed. In the last section, the surface analysis with XPS and the mechanism of the reaction are presented. Chapter 5 summarizes the results and presents the conclusions.

1.2 Orthodontic Materials

The first metal used for the fabrication of oral restorations was gold. The gold bridges were attached inside of the mouth using wires. Gold, as noble metal, is highly resistant to corrosion, has a good workability, it is biocompatible but aesthetical problems and the price made its use rare. Other metal alloys are thus preferred. In the seventies they were classified into *valuable*, for the most gold amount, and *non-precious* [11]. Gold was mixed with palladium and the materials were called semi-precious alloys. This terminology, however, identifies only alloys based on the cost of the elements and not based on the properties of the alloys themselves. Over the past 35 years, several factors have influenced the choice of the alloys used in orthodontics:

1. The large fluctuations and the consequent rise in prices, since the early seventies, caused a decrease in the use of precious metals such as gold, palladium, silver and platinum and alloys for prosthodontics restorations. [12].
2. The demand of alloys with improved mechanical properties strongly increased. It is acknowledged that gold-based alloys have an elastic modulus that is about half of that found in those on nickel- based ones.
3. The need of new materials with higher biocompatibility and corrosion resistance stimulated the research in this field. Over the past twenty years in fact these two properties have become very important as is the workability and esthetics.

In the field of dentistry four types of materials such as metals, ceramics, polymers and composites are used today. The choice of a type of material is not only governed by the physical and mechanical properties of the material but also by the purely esthetic needs. Plastic or ceramic materials are very attractive from the esthetic point of view, they possess mechanical deficits such as higher incidence of bracket fracture attributed to the lack of grain boundaries [13, 14]. Today in orthodontics cobalt-chromium alloys, stainless steels and titanium-based alloys are successfully used for the production of orthodontic brackets and wires. They are resistant to corrosion thanks to the presence of elements such as chromium and molybdenum that promote the formation of protective oxide layers that are almost insoluble in many body fluids at the physiological pH. To ensure corrosion resistance in the mouth, the content of chromium and molybdenum has to exceed 25 wt.%. Other elements like manganese, silicon, iron, tantalum, niobium, carbon, and nitrogen are needed for castability, weldability, and to improve other physical properties. The Co-Cr-Mo alloys were used instead of those containing nickel because the presence of nickel could

cause allergies. Cobalt-based alloys, however, have a high value of hardness and are not easily workable. Adding alloying elements such as gallium and indium, the workability is improved but at the cost of a significant decrease in corrosion resistance [11]. Today, low-nickel stainless steels and nickel-free stainless steels are introduced in orthodontics as alternative to conventional types of steel that contains nickel. Nickel is an element that, as amply demonstrated in the literature, causes allergies in susceptible individuals [15].

Titanium has been widely used to design dental implants because of its biocompatibility and corrosion resistance. Commercially pure titanium (CP-Ti) was initially used for biomedical applications, however, due to its low strength, difficulty in polishing, and poor wear resistance, other titanium alloys, like Ti6Al4V were developed [16]. The American Society for testing and Materials (ASTM) divides the CP Ti in five unalloyed grades (Grades 1-4, and Grade 7), depending on the concentration of oxygen (0.18 wt %-0.40 wt %) and iron (0.2 wt %-0.5 wt %). Titanium forms a stable and adherent thin protective titanium oxide layer on its surface, which spontaneously covers the metal surface and is around 1–4 nm thick. The stability of the passive film depends on its composition and structure, which are also dependent on the conditions under which it is formed.

1.3 Stainless steels

Stainless steels are frequently used in orthodontics and find application in other fields of dentistry. These materials are also used as bone implants due to their relatively low cost, excellent mechanical properties, good corrosion resistance and biocompatibility. Adding alloying elements such as chromium and nickel to iron the properties of the alloy are improved. The corrosion resistance of stainless steels depends on the spontaneous formation of a protective film, the passive film. This film has a thickness of a few nanometers and is mainly composed of Cr(III)oxy-hydroxides that prevent further dissolution of the alloy.

Crystal structure of stainless steels

There are three classes of stainless steels classified according to their crystal structure: ferritic, austenitic and martensitic. *Ferritic* stainless steels (iron chromium alloys) contain chromium in a range of 12% to 25%. The structure is body-centered cubic (BCC). Ferritic stainless steels do not

contain nickel. They exhibit superior corrosion resistance to martensitic stainless steels and possess good resistance to oxidation.

Austenitic stainless steels are the most corrosion resistance alloys and these steels are employed in orthodontic material, endodontic instruments and crowns in pediatric dentistry. The austenitic structure is face-centered cubic (FCC) [17,18] and is achieved by the addition of nickel to the iron-chromium alloy. Increasing chromium (and molybdenum) content requires a higher amount of nickel to preserve the austenitic structure.

Martensitic stainless steel may be heat-treated, as conventional steels, to provide a range of mechanical properties. They offer higher hardenability but the corrosion resistance is quite poor.

Austenitic-ferritic steels, called *duplex steels* have a mixed grain structure of austenite and ferrite. The chromium content ranges from 18 to 25%, nickel from 4.5 to 6.5%, an amount sufficient to get about 50% of the grains austenitic. Other alloying elements like molybdenum are added to improve pitting corrosion resistance in the range from 2 to 6 %.

Classification

The American Iron and Steel Institute (AISI) uses codes 200 and 300. The series 200 is used for austenitic chromium-nickel-manganese alloys and 300 for chromium-nickel alloys. AISI 304 is the most widely used austenitic steel also known as 18/8 for its composition of 18% chromium and 8% nickel. Ferritic and martensitic stainless steels are designated by a code 400 series. DIN (Deutsches Institute für Normung) uses five numbers, the first one separated by a dot: DIN 1.4456 where 1 means iron based alloys. European stainless steel classifies the steels names based on a chemical composition where at least one of alloy element has more than 5 percent by weight. The notation starts with a letter X followed by a number that represents the content (100 times larger) of carbon in the alloy; chemical symbols which many of the elements present and the numbers that indicate the value of their content. Therefore, X5CrNi18 -10 contains 0,05% C , 18% Cr , 10% Ni.

Effect of the alloying elements

Properties of stainless steels are due to the addition of alloying elements. *Carbon* content should be as low as possible in order to improve corrosion resistance and to avoid inter-crystalline corrosion. *Chromium* is the key element responsible for the corrosion resistance. The ease of formation of a passive film and the corrosion resistance are the direct result of the presence of chromium. If the content of chromium is at least 12%, an adherent and insoluble surface film is

spontaneously formed in rural, clean environments with neutral pH. More aggressive environments require increasingly higher chromium content to achieve passivation.

The presence of *nickel* results in the formation of an "austenitic" fcc structure that gives these grades their good ductility and toughness. Nickel usually is not present in the passive film but it is enriched in the alloy beneath the film [19,20,21].

Generally *manganese* is added to stainless steels for the powerful deoxidation capacity. The presence of manganese increases the hardenability of the steel. Manganese is also an austenite stabilizer and when added in higher amounts (from 4 to 18%) replaces nickel in the 200 series stainless steel grades [22].

Small percentages of *molybdenum* have powerful effects in improving the resistance to pitting corrosion in chloride bearing environments and to crevice corrosion in both Fe-Cr alloys and Fe-Cr-Ni alloys. Molybdenum reduces critical current density for passivation, thus improves passivation and decreases the tendency of the passive films to break down.

Nitrogen in austenitic and duplex stainless steels increases the resistance to localized corrosion. Nitrogen is an interstitial element in steel because its atomic size is sufficiently small to allow this element to enter the α-alloys and the γ-alloy lattices as interstitial atoms.

Biocompatibility

The traditional austenitic alloys containing nickel create problems of biocompatibility. As is well known, nickel causes allergies in susceptible individuals with genotoxic and carcinogenic effects [23]. Considering that both orthodontic appliances and orthopedic implants are in contact with the body fluids for long periods it was therefore necessary to develop more biocompatible stainless steels. The nickel-free austenitic steels have been produced to give a valid answer to this problem. Nickel is replaced by manganese, which equally promotes the formation of the austenitic structure [24]; another alloying element used in stainless steels is molybdenum that modifies the passive film making it more stable in presence of chloride ions that cause the formation of pits on the surface. Various theories have been proposed to explain the influence of molybdenum. Some authors assert that Mo has influence on more than one step in a pitting event. Thus, during formation of pits, the molybdenum acts forming insoluble compounds, generally MoO_3 covering the walls of the hole, favoring the repassivation and the deactivation of the growing pits [9]. Several studies on the biocompatibility of stainless steels were made using synthetic fluids in order to reproduce an environment like the real one. The human body in fact, is not a pure saline

environment but also contains proteins that are capable of binding metal ions. One study reports the effect of complexing agents in physiological solutions on the formation of the passive film and how the presence of molybdenum could further influence the behavior of these steels. Indeed it has been reported that the presence of complexing agents such as citrate acts on the formation, composition and properties of the passive film. The composition and the thickness of the surface film were evaluated by X-ray photoelectron spectroscopy. It results that the passive film is composed of chromium and iron oxy-hydroxides and in minor amounts oxides of Ni and Mo. An enrichment of oxides of molybdenum and depletion of chromium and iron at the film-bulk interface was reported. It was also demonstrated that the thickness of the passive film in the presence of citrate is thinner than that formed in physiological solution without citrate. The presence of complexing agents thus changes the composition of the metal beneath the passive film [25].

Nickel-free stainless steels

In recent years nickel-free stainless steels with high nitrogen content have been developed. It has been documented in previous studies that nitrogen has a beneficial effect on corrosion resistance. Wan et al. [26] reported a study conducted on a nickel-free stainless steel with various concentrations of nitrogen and the effect of proteins through electrochemical experiments. The results of this study showed that the increase of nitrogen content promotes the formation of a thicker and more protective oxide film. The study carried out using solutions of albumin and fibrinogen showed how proteins play a key role in the formation of the film because they are complexing agents. In fact, in this study both platelet adhesion on the surface and the tendency of blood to clot was compared with standard steel (AISI 317L). The result of platelet adhesion was observed by SEM images; platelet adhesion decreased with increasing nitrogen content. This behavior may be explained by considering the theory of some authors according to them the nitrogen content increases the concentration of free electrons. The surface then acquires a negative charge when compared with AISI 317L and considering that the blood platelets they also have a negative charge, it could explain the difficulty of platelets to adsorb on the surface.

1.4 Biocompatibility and development of new materials

The biocompatibility of a material is a complex property. When a material comes into contact with body fluids an interface is created that is normally not present. This interface is not static but there are dynamic interactions. The material interacts with the body and the body's response to this interaction can be quite different. The biocompatibility, therefore, depends on a variety of conditions, such as material properties and the context in which the material is placed. The biological responses are classified as toxic, inflammatory, allergic reactions and mutagenic.

The residence time of a material in the body is important for the biological response; materials that are only present for 1 hour in the oral cavity produce a different response from those materials that will remain for years. Thus, the residence time is an important factor because some effects due to the interaction between the material and the body develop only in the long term. The materials can release substances that in a certain concentration can be toxic to the body.

Allergies and inflammation may be the result of the toxicity of a material. Some materials such as latex are responsible for allergic states through the contact with the material. An allergic response occurs when the body's immune system does not recognize a substance as its own.

Three types of tests are used to measure the biocompatibility of new dental materials: in vitro, animal and usage test. Generally, these tests are performed together to evaluate the biocompatibility of new materials. First tests are performed in vitro, for example in vitro cytotoxicity and mutagenicity [23] tests to evaluate a new alloy. The testing of a new material is a linear progression from primary to secondary to usage tests and only materials that have passed the primary stage can switch to secondary and only those who have passed the secondary stage pass to usage tests. The secondary tests are almost always conducted in animals, but animal tests are expensive and difficult to control. These tests are also controversial because they represent an ethical problem. Thus more sophisticated in vitro tests are being developed that can replace animal tests. Usage tests are performed in animals or humans. Animals for usage tests are limited because animals are not employed for all clinical situations due to a size or anatomy of a given species. If the usage tests are carried out on humans is necessary to obtain the authorization by law of an “Ethics Committee”, in USA is an Institutional Review Board.

Nickel allergy

An allergic response occurs when the body's immune system does not recognize a substance as its own. The release of metal ions into the tissues can create severe inflammations. An example is nickel that, as already mentioned, is a component in the alloys used for the production of dental materials. Allergies and inflammation may be the result of the toxicity of a material. Some materials such as latex are responsible for allergic states through the contact with the material. Nickel is considered the most allergenic metal [27], and the incidence of allergies among men and women was very high, most likely for women considering the use of jewelry.

1.5 Corrosion of orthodontic materials

Biocompatibility of dental material is now a fundamental requirement of successful clinical behavior in oral cavity. There are two key factors that appear to be important in determining biocompatibility of any dental material, some involve various types of corrosion or material degradation and others include surface characteristics. Dental materials within the mouth are constantly interacting with biological fluids. Saliva is a hypotonic solution containing bio-actonate, chloride, potassium, sodium, nitrogenous compounds and proteins. Human blood contains chloride, potassium, sodium, magnesium, calcium, phosphates and hydrogen carbonate ions [28].

The chemical environment of blood plasma is highly aggressive for many metals and alloys, due especially to the presence of a quite high concentration of chloride ions and their ability to induce localized corrosion (pitting corrosion).

Corrosion is the gradual degradation of the material due to an electrochemical attack, and becomes of extreme importance when orthodontic appliances are placed in the hostile electrolytic environment provided by the human mouth [29].

An important requirement of a metal used as a dental material is that it does not produce harmful corrosion products to the body. The oral cavity is warm and moist, and is continually subjected to fluctuations in temperature, thus, factors such as temperature, quantity and quality of saliva, plaque, pH, proteins, physical/chemical properties of solids/liquids food and oral conditions may influence corrosion processes [30]. Various types of wires and brackets are used in the treatment of malocclusion e.g. stainless steel, cobalt-chromium-nickel alloys, nickel-titanium alloys, β-titanium alloys, etc [12]. Resistance to corrosion is very important for orthodontics because

corrosion can lead to roughening of the surface, weakening of the appliances, and release of elements from the metal or alloy.

Corrosion mechanism

When a metal is placed in contact with oxygen and water it will corrode and has the consequent formation of corrosion products. At the anode the alloy dissolves (oxidation reaction) according to

$$M^0 \rightarrow M^+ + e^-$$

At the cathode, reduction reactions must occur that will consume the electrons produced in the oxidation reaction:

$$O_2 + 2H_2O + 4e^- \rightarrow 4OH^- \qquad \text{in neutral media}$$

$$2H_3O^+ + 2e^- \rightarrow H_2 + 2H_2O \qquad \text{in acidic media}$$

The Pourbaix diagrams provide information about the stability of a metal and its oxides for different conditions of pH and potential. Figure 1.1 shows the diagram E vs pH of iron. The dashed lines ***a*** and ***b*** represent the two cathodic processes, reduction of protons and oxygen reduction.

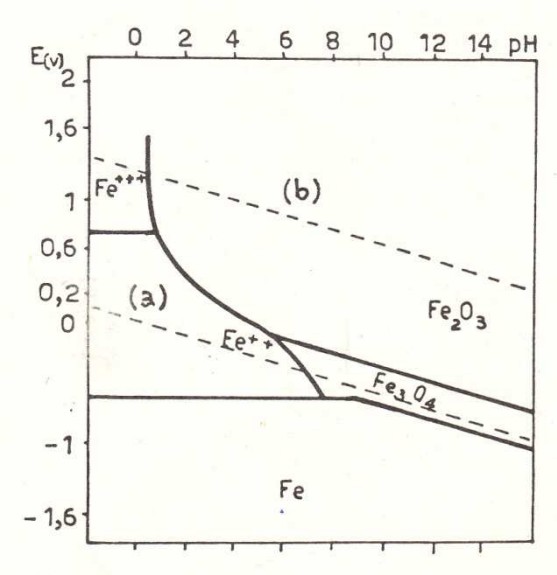

Figure 1.1 Pourbaix diagram of iron [31].

1.6 Types of corrosion

Uniform or general corrosion [32] occurs on the entire surface of the material exposed to the environment leading to a relatively uniform loss of thickness. Uniform corrosion is common for non-noble metals such as zinc or iron that cannot form a passive film [33]. The corrosion process begins with the interaction of the metal with the environment that causes the formation of hydroxides. The corrosive environment must have the same access to all parts of the surface and the composition must therefore be uniform.

Pitting corrosion is the most dangerous and troublesome corrosion attack that creates holes on the surface of the exposed material. Pitting corrosion occurs only on metals and alloys that form spontaneously a protective oxide layer on the surface. To trigger pitting corrosion chloride ions have to be present in the environment. In the initial stage of pitting corrosion chloride ions penetrate into the passive film at irregularities of the oxide film, first thinning of the passive film and the subsequent destruction. The size of the pits can vary from a few nanometers to the micrometer range. During the propagation stage the metal cations deriving from the anodic reaction have to be hydrolyzed in the pit environment. The pit environment becomes more acidic, leading to very aggressive conditions in the pit. Figure 1.2 shows the pitting mechanism.

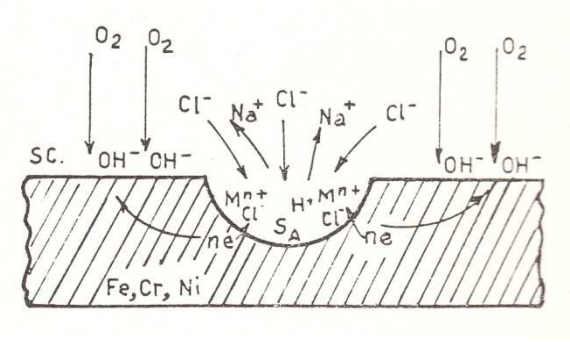

Figure 1.2 Pitting mechanism [31]

Pitting corrosion can be reduced by adding alloying elements such as Molybdenum [9,34].

Crevice corrosion is a type of localized corrosion that occurs between two surfaces in very close contact where there is little exchange of solution and oxygen is depleted. Oxygen is necessary for the formation of the passive film and for repassivation and repair. In the crevice the concentration of metal ions due to the corrosion process increases. To maintain neutrality chloride ions are diffusing into the crevice. As a consequence in a crevice the pH will be in a range of pH about 4 [35].

Fretting and erosion-corrosion occurs when there is a movement between two metal surfaces immersed in a corrosive fluid. In cases where the material is exposed to mechanical wear, the

protective film present on the surface is locally removed, exposing the active surface of the metal. Fretting corrosion occurs due to the combined action of mechanical and chemical attack. The absorption of the metals by the tissues is usually due to this type of corrosion.

Intergranular corrosion is a form of localized attack that occurs along the grain boundaries of a metal. Intergranular corrosion leads to a drastic loss of the mechanical resistance and ductility. When the intergranular attack is severe, the grains can be separated from the matrix, in which the metal crumbles and loses consistency. Austenitic stainless steels are susceptible to intergranular corrosion when heated in a range between 400 and 850 ° C [35]. When they are heated in this temperature range for a sufficient time, chromium and carbon precipitate from the solid solution and are forming chromium carbides at the grain boundaries. If the concentration of carbon in the steel is less than 0.03 % (stainless steels L-series, or low carbon) the precipitation of chromium carbide is retarded and the stainless steel remains immune to intergranular corrosion.

Galvanic corrosion occurs when two materials having a different electrochemical potential (or two parts of the same material that are exposed to different conditions), are placed in direct contact (forming a galvanic coupling) in an electrolyte. In orthodontics this type of corrosion occurs when two different materials are placed in contact as in the bracket and the arch wires. The ratio of the areas of the two metals or alloys is very important because it affect the corrosion process. If the area of the anode is very small compared to that of the cathode, the rate of dissolution of the anode is very fast.

Stress Corrosion Cracking (SCC) is a phenomenon of degradation of a material due to the combined action of corrosion and application of a constant load. Often leads to unexpected rupture of ductile metallic materials normally subjected to stress in a corrosive environment, especially at elevated temperatures. The speed of propagation of the fracture is considerable precisely because of the combined action of the two factors. Thus, an electrochemical potential difference occurs with specific sites acting as anodes and other surfaces acting as cathodes. This type of corrosion occurs even in orthodontic wires. The NiTi alloys remaining for many months in the oral cavity, suffer from this problem [35].

1.7 Corrosion of stainless steel

Stainless steels are used in orthodontics because they have good mechanical properties and excellent corrosion resistance. In particular, steels with austenitic structure have a high resistance to corrosion compared to other steels with ferritic and martensitic structure. As mentioned

previously, the corrosion resistance is due to the formation of a protective passive film thanks to the presence of chromium in the alloy. Austenitic stainless steels are usually alloy with Ni, for example 18Cr-8Ni (DIN 1.4301) and 316L that contain a small amount of molybdenum to improve the strength and corrosion resistance [5, 36]. Several studies have shown that the passive films is formed by a layered structure with an inner part of Cr_2O_3 and an outer part iron and nickel oxy-hydroxide at the film-electrolyte interface [25].

Influence of fluoride ions

Brackets and orthodontic wires are continuously stressed by physical and chemical changes within the oral cavity such as temperature variation, variation of the composition of saliva, ingestion of food during meals. Usually the presence of orthodontic appliances in the oral cavity forces to have a greater dedication in cleaning the teeth, through the use of specific mouthwashes, dental floss, toothpaste, because the presence of a temporary appliance makes this operation difficult and avoids irritations. The use of these products is therefore recommended to reduce the risk of dental caries. However, several studies have shown that in an acidic environment and in the presence of fluoride ions the corrosion resistance of the materials used in orthodontics may become worse. The protective passive film on the surface of the material can deteriorate in the presence of fluoride ions. Schiff et al. [37] studied some materials (cobalt-chromium, iron-chromium-nickel and titanium) used in orthodontics put in contact with three types of mouthwashes containing fluoride. Polarization resistance and microstructural analysis by SEM showed that the titanium alloy and Fe-Cr-Ni had the same corrosion resistance. The polarization resistance of these two materials is very low in one of these mouthwashes containing stannous fluoride. In fact, this ingredient causes both in the Fe-Cr-Ni alloy as in titanium the progressive destruction of the passive film. These findings were also confirmed by SEM that showed for the alloy Fe-Cr-Ni intergranular corrosion [37]. Similar results were obtained also in the work of [8], which studied the change in the surface characteristics and corrosion of stainless steel and NiTi alloys immersed in artificial saliva in presence of NaF. SEM micrographs showed surface defects in the steel and the presence of localized corrosion. As mentioned previously, chloride and fluoride ions penetrate the passive film triggering points of localized corrosion. The degradation of a material can be accelerated when the surface presents irregularities due to the steel production process, but also by the forces applied by the orthodontist in the moment in which the device is mounted inside the mouth of the patient. In these conditions, the steel can be subject to crevice corrosion. Food debris that are trapped in the brackets and the plaque bacteria play a very

important role as the products resulting from the metabolism of the bacteria favor a decrease in pH. The decrease in pH contributes then the triggering of the corrosion process. [2].

Influence of molybdenum

Pitting corrosion can be limited by the presence of molybdenum in the alloy. A study [9] shows the mechanism by which the molybdenum would act as a protector in the nucleation phase of the pits. A multi-stage mechanism in which Mn and Mo participate in pitting corrosion behavior of the austenitic stainless steel is proposed. Considering that manganese has a strong affinity to sulfur it forms MnS easily. MnS are considered preferential initiation points of pitting corrosion [38,39].

Another study shows [40] polarization curves performed on stainless steel AISI 304L and AISI 316L immersed in a 5% of NaCl aqueous solution. In the passive region, the current density is lower in AISI 316L than for AISI 304L indicating the influence of molybdenum. XPS spectra revealed the presence of Mo (IV) forming MoO_2 and of chloride but no signal for sodium, which indicates that the chlorine is not bound to sodium in NaCl. It is concluded that Mo forms complexes with chlorine, consequently less chlorine is introduces into the passive films during its formation and growth.

1.8 Methods for investigating the stability of orthodontic materials

Several techniques are used to evaluate the stability of orthodontic materials, pointing on the biocompatibility of the material and its corrosion resistance. In this thesis, the evaluation of the biocompatibility of the nickel-free stainless steel was performed using electrochemical techniques to evaluate the corrosion behavior and the corrosion rate of the stainless steel in artificial saliva. In addiction surface analysis by X-ray photoelectron spectroscopy has been performed. This technique allows obtaining information about the composition and thickness of the passive film. Contact angle measurements have been performed to evaluate the wettability of the surface after contact with artificial saliva for different immersion time.

1.8.1 Electrochemical techniques

Electrochemical techniques are frequently employed to estimate the in vitro corrosion behavior of dental alloys. Several electrolytes like saline solution with appropriate chloride ions concentrations or artificial saliva that simulate the oral cavity are used (Fusayama, Ringer solution etc.). Moreover, in in vitro tests usually are performed at body temperature (37 °C). The alloy is put in contact with the test solution in an *electrochemical cell*. Three electrodes are required to perform the experiments: a *working electrode* (the steel plate in this work), a *counter electrode* (ordinarily platinum) and a *reference electrode* (usually a saturated calomel electrode or a saturated Ag|AgCl electrode). A potentiostat connected to a computer is used to control the experiment.

Open Circuit Potential (OCP) measurements show the variation of the potential of the material placed in contact with a test solution (e.g. artificial saliva) versus time. The potential of the steel (working electrode) is relative to a reference electrode. The variation of the potential of the sample is plotted versus time and it is possible to distinguish if the samples corrode (potential become more negative) or form a passive film on the surface (the potential tends asymptotically to positive values). Figure 1.3 shows an example of a nickel-free steel immersed in artificial saliva at body temperature of 37 ° C shows this behavior.

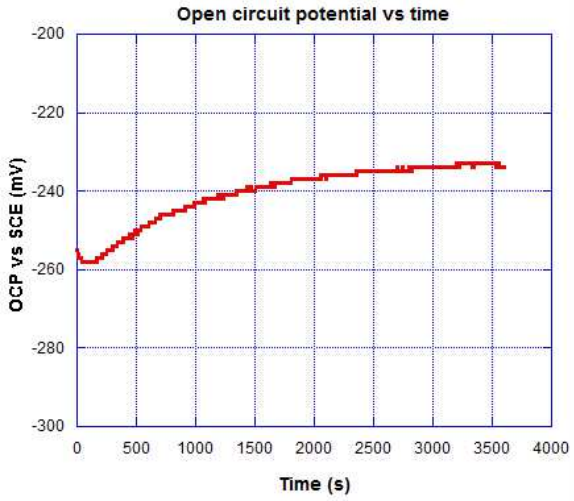

Figura 1.3 OCP of Stainless steel in artificial saliva

Potentiodynamic polarization curves allow to obtain information about the ability of a material to passivate in a given environment, the potential range in which the material is in a passive state or the corrosion rate in the active state. Experimentally the polarization curve is obtained by plotting the current that is obtained as a function of the applied potential. The behavior of a metal in a

given environment can be monitored by means of this diagram. A typical polarization curve for a metal in a passive state is shown in Figure 1.4 and figure 1.5. The anodic curve (fig. 1.4) and the cathodic curve (figure 1.5) obtained for a nickel-free steel in artificial saliva can be described as follows:

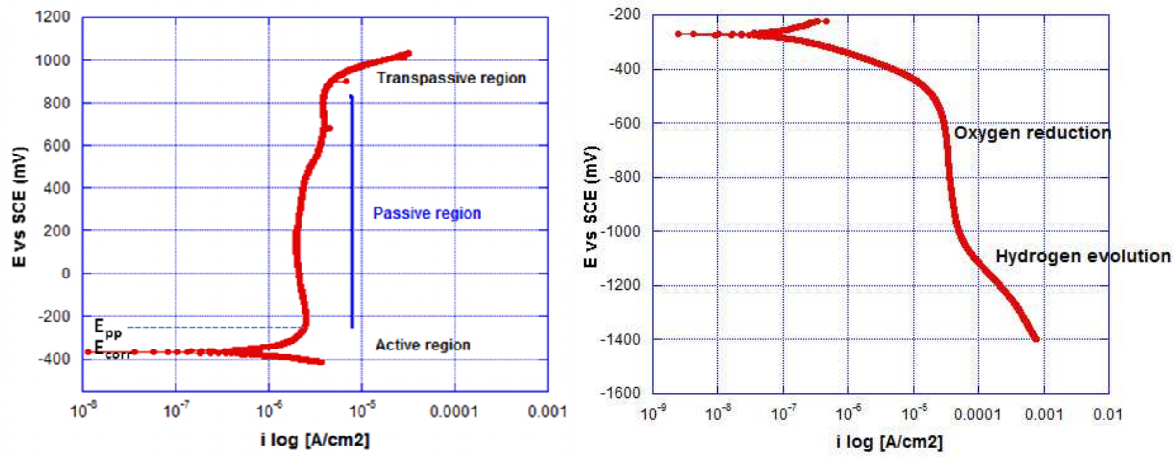

Figure 1.4 and figure 1.5 Anodic (left) and cathodic (right) curve for a nickel free stainless steel immersed in artificial saliva

A*ctive region:* between E_{corr} and E_{pp} (primary passivation potential) the metal is in a state of active corrosion, the corrosion current increases exponentially. At E_{pp}, the current reaches its maximum and then begins to decrease. The metal is in the *passive state*, constituted by the formation of a passive film that prevents further corrosion of the metal. In this phase the current has very low values but the film formed is in continuous evolution, consisting of stages of dissolution together with stages of repassivation. The diagram also shows a *transpassive region* in which the current increases again rapidly to more positive potentials and the passive film is destroyed. The cathodic polarization curve (figure 1.5) illustrates instead a zone of stability, between -500 to -1000 mV SCE due to the *oxygen reduction* and at -1000 mV the current density increases accompanied by the *hydrogen evolution*.

The **Polarization resistance** technique is used to evaluate the corrosion rate. Polarization resistance measurement consists in a potential scan of ±20 mV versus E_{corr}, the corrosion potential. The resulting current is plotted as a function of applied potential. It follows that:

$$\frac{\Delta E}{\Delta i} = \frac{\beta_A \beta_C}{2.3(i_{corr})(\beta_{A+}\beta_C)}$$

where ΔE /Δi is the slope of the Polarization Resistance and β_A and β_C are anodic and cathodic Tafel constants, i_{corr} is the corrosion current.

$$\frac{\Delta E}{\Delta i} = \frac{1}{Rp}$$

From the polarization resistance Rp (Ωm^2) the corrosion current density i_{corr} can be calculated.

$$i_{corr} = \frac{B}{Rp}$$

where the constant B is related to β_A and β_C by following equation:

$$B = \frac{\beta_A \beta_C}{2.303(\beta_A + \beta_C)}$$

B has a value of 52 mV for steel in passive state.

1.8.2 X-ray photoelectron spectroscopy

X-ray photolelectron spectroscopy is an analytical technique that is based on the photoelectric effect. It is surface sensitive and it is used in various research fields as in the study of corrosion of materials, microelectronics, catalysis, tribology, and many others. It is acknowledged that since the surface of a material is in direct contact with the surrounding environment and has different properties than the bulk, it is necessary to know its composition, concentration and chemical state of the elements present and thicknesses of the films eventually formed on it. XPS is therefore a powerful technique suitable for the purpose.

XPS is based on the ejection of an electron from either a core or from a valence level of an atom by absorption of photons of suitable energy, X. The kinetic energy KE of the emitted electrons is measured by the spectrometer, and depends on the energy of the X-ray used, therefore, is not an intrinsic property of the material. The binding energy of the electron (BE) instead identifies a particular atom. These terms are related by the equation [41]:

$$KE = h\nu - BE - \phi$$

Where KE is the photoelectron kinetic energy; BE is the electron binding energy in the solid; Φ is work function of the analyzer also known as spectrometer work function; hν is the energy of the X-ray source used. Φ is the work necessary to remove the electron from the material and bring it to the vacuum level.

In order to have photoemission is necessary that the energy of the incident beam X is greater than the binding energy of the electron. Figure 1.6 shows the ejection of an electron from the K level thanks to the energy absorption of the incident X-ray beam and the consequent creation of a hole.

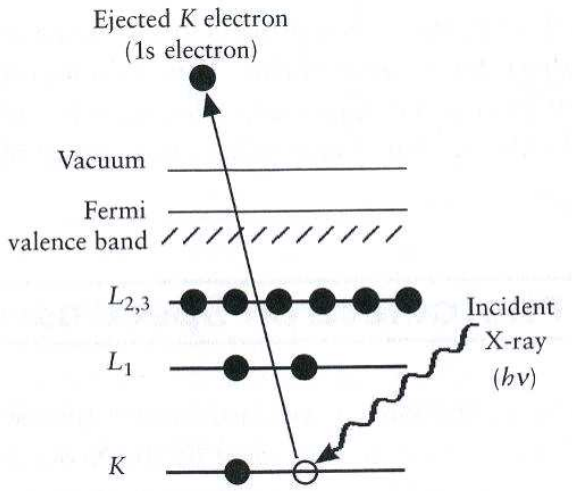

Figure 1.6 Scheme of photoionization of atoms [41]

Since only the electrons originating from the outer part of a solid are able to reach the detector without losing energy, XPS is considered a surface sensitive technique.

The average distance λ (nm) traveled by an electron without undergoing inelastic collisions is the *inelastic mean free path* and there are several ways to calculate it in the literature [42]. The simplest approach was proposed by Seah and Dench [43]:

$$\lambda = A * KE^{-2} + B * \sqrt{KE}$$

Where A and B are two parameters that depend on the type of material. If the kinetic energy KE of photoelectrons is between 150 and 2000 eV, the first term of the relationship is negligible compared to the second and the relationship may take the form:

$$\lambda \cong B * \sqrt{KE}$$

The photoemission process involves the formation of a hole and an ionized atom. The atom relaxes in two possible ways with the emission of a secondary electron, called Auger electron or by X-ray fluorescence. The two processes are simultaneous and in competition and depend on the atomic number Z of the element. The identification of the elements is obtained by recording the energy distribution of photoelectrons emitted as a function of binding energy, for a given angle of emission. Usually the spectrum has a very wide energy range (from 0 to 1400 eV) and it is called the *survey scan or wide scan*. The electronic energy is determined by different terms that take into account the motion of the electron around the nucleus, the nucleus – electron interaction, the electron – electron repulsion and the so-called exchange term. The fact that different nuclei have different positive charge implies that the electrons have different binding energies going from one

element to the next one. This makes XPS a technique that allows the peak identification on the basis of the binding energy values of the photoelectron signals. Only *certain values* of electronic energy are allowed for an atom said to be ***quantized***; a change of electronic energy level (state) of an atom involves the **absorption** or **emission** of a definite amount, quantum, of energy. The lowest electronic energy state is called the **ground state**, while any state with energy greater than that of the ground state is an **excited state**. Furthermore, in the spectrum is possible to verify the presence of multiple peaks associated with a specific element corresponding to the electronic configuration of the electrons in the atom. The peaks corresponding to the core levels are generated by the ionization of electrons from the core levels of the atom and may have a fine structure characterized by the coupling spin - orbit. The electrons that during the process of photoemission lose energy due to the inelastic scattering contribute to the background.

In addition to the qualitative analysis, i.e the identification of the elements present in the material under study, it is possible to evaluate the chemical state of the elements. Indeed, the binding energy of an electron depends not only on the level from which the electron is ejected, but also on the oxidation state of the atom and from chemical and physical environment in which it is located. Variations of these two factors produce small shifts of the peaks in the spectrum, and this effect is called *Chemical Shift*.

The interpretation of the signals is made by comparing the spectra recorded with those obtained on the reference compounds in the same experimental conditions. Tables with the positions of the signals for the different chemical states can be found in the literature [44].

High-resolution spectra that allow the identification of the chemical state of the elements can also be recorded. Quantitative analyses of the surface layers can be performed using the area of the peaks that is directly related to the concentration of the elements in the solid. The composition and the film thickness can be calculated by means of the *three-layer model* [45] that considers the surface divided into three layers: an outer layer of contamination, an intermediate layer of oxides and hydroxides, and a substrate interface film / substrate. The model assumes homogeneity of the layers.

Contact angle is a surface characterization technique complementary to XPS and SIMS. It provides information about interaction of liquid with a solid. The contact angle measurements therefore allow a better understanding of these interactions. Medical, pharmaceutical and cosmetic industries also use contact angle measurements in their research and quality control laboratories. Biomaterials are employed to create disposable lenses, catheter, and dental materials, body

implants; therefore they must be biocompatible and should not be rejected by the human body. Some fields which are used in the contact angle measurements are those of research on products for personal hygiene care of babies, for example diapers super absorbent, or creams or powders talc used to decrease the moisture of the skin. Shampoo, body cream, skin solution, lotion and other are employed to test with contact angle measurements in the cosmetic industry. As it has been already mentioned, the biocompatibility is a very important requirement in the medical and dental industries. Thus, contact angle measurements are essential in all wettability and biocompatibility studies.

The contact angle is a quantitative measure of the wetting of a solid by liquid. If consider a liquid drop resting on a solid, the drop remain in equilibrium due to the balance of the three forces, interfacial tension between the solid and liquid SL, between liquid and vapor LV and between solid and liquid SL. The figure below shows the balance between the three forces.

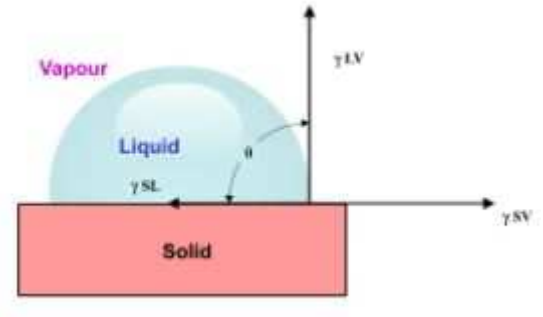

Figure 1.6 Balance between the three forces-Young equation [46]

Low values of contact angle indicate a high surface wettability and a strong interaction between solid and liquid, while high values of contact angle indicating a weak interaction liquid-solid. If θ is less than 90° the surface of the solid is defined *wet* or *partially wet.* At *zero* contact angle the surface is *complete wetting. I*f theta is greater than 90 ° the surface is considered non *wetting* (figure 1.7).

Figure 1.7 Contact angle on different materials [47]

The vectorial sum of these three forces was explained by Young equation [48]:

$$\gamma_{SV} = \gamma_{SL} + \gamma_{LV} cos\theta$$

Where γ is the surface tension

There are various methods to measure the contact angle, one of the most widely used involves the use of a goniometer and thanks to the video camera and a magnifying lens equipped it reproduces the image of the drop (Drop Shape Analysis). It is possible then to determine the value of the tangent graphically. It is not possible, however, to determine in an exact manner the value of the contact angle with a single measurement. Young's law can be applied only to ideal solid that are chemically homogeneous, flat and cleaned. Rather the surface of a solid is not homogeneous and presents irregularities.

References

[1] W. D. Mueller, C. Shoepf, M. L. Nascimento, A.C. Carvalho, M. Moisel, A. Schenk F. Scholtz, K.P. Lange, Electrochemical characterization of dental alloys: its possibilities and limitations, *Anal. Bioanal. Chem.* (2005) 381: 1520-1525

[2] J. Daems, J.P. Celis, G. Willems, *European Journal of Orthodontics,* 2009, Vol. 31, 260–265

[3] D. D. Upadhyay, M. A. Panchal, R.S. Dubey, V.K. Srivastava, *Materials Science and Engineering A* 432 (2006) 1–11

[4] J.C. Wataha, *The Journal of Prosthetic Dentistry*, 2002, Vol. 87, Issue 4, 351–363

[5] D. Kuroda, T. Hanawa, S. Hiromoto, Y. Katada, K. Asami, *Materials Transactions*, 2002, Vol. 43, No. 12, 3093-3099

[6] E. A. Vogler, *Journal of Electron Spectroscopy and Related Phenomena*, 81 (1996) 237-247

[7] A. Madureira Barcelos, A. S. Lunaa, N. de Assis Ferreira, A. V. Castro Braga, D. C. Baptista do Lagoa, L. Ferreira de Senna, *Materials Research*, 2013, 16(1): 50-64

[8] C.-Tze Kao, T.-Hsien Huang, *European Journal of Orthodontics* 32 (2010) 555–560

[9] A. Pardo, M.C. Merino, A.E. Coy, F. Viejo, R. Arrabal, E. Matykina, *Corrosion Science*, (2008), Vol. 50, 1796–1806

[10] G. Tani, F. Zucchi, Electrochemical Evaluation of the Corrosion Resistence of Commonly Used Metals in Dental Prosthesis, *Minerva Stomatol.* 1967, 16, 710-713.

[11] W. Braemer, *Advanced Engineering Materials*, 2001, 3, No. 10

[12] J.C. Wataha, *The Journal of Prosthetic Dentistry*, 2002, Vol. 87, Issue 4, 351–363

[13] VV. AA, Phillip's *Science of Dental Materials*, Elsevier, 2003

[14] T. Eliades, *American Journal of Orthodontics and Dentofacial Orthopedics*, 2007, Vol. 131, No 2

[15] R. Matos de Souza, L. Macedo de Menezes, *Angle Orthodontist*, (2008), Vol. 78, No 2

[16] M. P. Licausi, A. Igual Muñoz , V. Amigó Borràs, *Journal of Physics D: Applied Physics*, 2013, Vol. 46

[17] *W. F. Smith,* Scienza e tecnologia dei materiali*, 2ª ed., McGraw-Hill, 1995.*

[18] K.H. Lo, C.H. Shek, J.K.L. Lai, *Materials Science and Engineering* (2009), Vol. 65, 39–104

[19] D. Addari, Nanosized films on the surface of stainless steels. PhD Thesis, Università degli studi di Cagliari, 2005

[20] D. Addari, B. Elsener, A. Rossi, *Electrochimica Acta* 53 (2008) 8078- 8086

[21] A. Rossi. B. Elsener, *Materials and Corrosion* 2012, 63, No. 9999

[22] http://www.euro-inox.org/14-01-2014

[23] M.T. Costa, M.A. Lenza, C.S. Gosch, I. Costa, F. Ribeiro-Dias, *Journal of Dental Research*, (2007), Vol. 86, 441-445

[24] J.R. Davis, ASM Speciality Handbook, Stainless Steel, ASM International, 1994, p.22

[25] I. Milosĕv H.-Henning Strehblow, *Journal of Biomedical Materials Research*, 2000, Vol. 52, Issue 2, 404–412,

[26] P. Wan, Y. Ren, B. Zhang, K. Yang, *Materials Science and Engineering*, 2012, C 32 510–516

[27] L. M. Menezes, L. C. Campos, C. C. Quintão, A. M. Bolognese, *American Journal of Orthodontics and Dentofacial Orthopedics*, Vol. 126, Issue 1, 58–64

[28] Oyane A, Kim HM, Furya T, Kokubo T, Miyazaki T, Nakamura T., *J Biomed Mat Res* 2003; 65A:188–95

[29] S. Virtanen, I. Milosĕv, E. Gomez-Barrena, R. Trebsĕ, J. Salo, Y.T. Konttinen, *Acta Biomaterialia* 4, 2008, 468–476

[30] T.P. Chaturvedi, Corrosion behavior of orthodontic alloy-a review, *The Orthodontic Cyber Journal*, 2008

[31] G. Bianchi, F. Mazza, "Corrosione e Protezione dei Metalli", 3a edizione, Masson Italia Editori, Milano, 1989

[32] X. Q. Wu, S. Xu, J. B. Huang, E. H. Han, W. Ke, K. Yang, Z. H. Jiang, *Materials and Corrosion* 2008, Vol. 59, No. 8

[33] V. Cicek and B. Al-Numan, *Corrosion Chemistry*, 2011, John Wiley & Sons

[34] K. Hashimoto, K. Asami, A. Kawashima, H. Habazaki, E. Akiyama, *Corrosion Science*, (2007), Vol. 49 42–52

[35] TP Chaturvedi, *Indian J. Dent. Res*., 2010, 21 (2)

[36] C.-O.A. Olsson , D. Landolt, *Electrochimica Acta* , 48 (2003) 1093_/110

[37] N. Schiff, F. D. M. Lissac, L. Morgon, B. Grosgogeat, *European Journal of Orthodontics*, 2005, 27, 541–549

[38] N. Hara, K. Hirabayashi, Y. Sugawara, I. Muto**,** *International Journal of Corrosion*, 2012Vol. 2012

[39] A. Rossi, B. Elsener, G. Hähner, M. Textor, N. D. Spencer, Surface and Interface Analysis, 29, 460–467 (2000)

[40] J.M. Bastidas, C. L. Torres, E. Cano, J.L. Polo, Corrosion Science, 2002, Vol. 44, 625-633

[41] J. F. Watts, J. Wolstenholme, An Introduction to Surface Analysis by XPS and AES, WILEY, 2003

[42] S. Tanuma, C.J. Powell, D. R. Penn, Surface and Interface Amalysis, 36 (2004), 1-14

[43] M.P. Seah and W.A. Dench, Surface and Interface analysis, 1 (1979), 2-11

[44] D. Atzei, B. Elsener, A. Rossi , Atti del Congresso XIX Congresso di Chimica Analitica, 11 – 15 Settembre 2005 Università degli Studi di Cagliari, Centro Polaris, Pula (Sardegna)

[45] A. Rossi and B. Elsener, Surface and Interface Analysis, 18 (1992) 499 – 504

[46] https://www.smitherspira.com/testing/material-properties/paper/Water-Drop-Contact-Angle-WDCA.aspx (14-01-2014)

[47] http://www.kruss.de/services/education-theory/glossary/contact-angle/ (14-01-2014)

[48] H. Y. Erbil, Surface Chemistry Of Solid and Liquid Interfaces, 2006, Blackwell Publishing

2 Experimental

2.1 Materials

Samples of nickel-free stainless steel, DIN 1.4456, have been investigated in this work. The solution used for the electrochemical tests was the artificial saliva made following "modified- Tani Zucchi" composition [1] to reproduce the oral environment. The structure of the steel was examined at the optical microscope after attack with the "Beraha's reagent" [2,3].

2.1.1 Reagents and Solutions

The chemical composition of the "modified -Tani-Zucchi" artificial saliva is provided in table 2.1

Name of the reagent	Description
KSCN	ACS reagent pure for analysis ≥ 99.0%
$NaHCO_3$	ACS reagent, 99.7-100.3%
NaH_2PO_4	BioXtra ≥ 99.0%
KCl	BioXtra ≥ 99.0%
CH_4N_2O	Bioreagent for molecular biology, suitable for cell culture
α-amilase	From human saliva Type IX-A– Sigma Aldrich

Tab. 2.1 Reagents used to prepare "modified Tani-Zucchi" artificial saliva

The reagents used for the preparation of the artificial saliva were supplied by Sigma Aldrich (Sigma-Aldrich S.r.l. Milan, Italy);

bidistilled water with specific conductivity of 1.1 µS/cm was used to make up the solutions.

Beraha's solution used for the color etching was made of:

HCl (37%) supplied by Carlo Erba (Italy) 20 cm^3,

Potassium metabisulfite 97% extra pure supplied by Acros Organics (pat of Thermo Fisher Scientific, Milano) 1g,

bidistillate water 100 cm^3,

Absolute ethanol 98% supplied by Carlo Erba (Italy)

2.1.2 Stainless steel

The samples used for electrochemical analysis and surface analysis were nickel-free stainless steels plates DIN 1.4456 with size of 200mm*200mm*0.8mm. The chemical composition is shown in table 2.2

Fe	Cr	Mn	Mo	N	C	S	Si
60.1	17.9	18.4	1.9	0.8	0.06	0.04	0.9

Tab. 2.2 Chemical composition of the Ni-free stainless steel

2.1.3 Mechanical polishing

The procedure provided by Struers [4] has been here followed for polishing the sample surface prior the electrochemical tests. Struers assembles the materials in a Metalogram (fig. 2.1) that shows them according to specific physical properties: hardness and ductility.

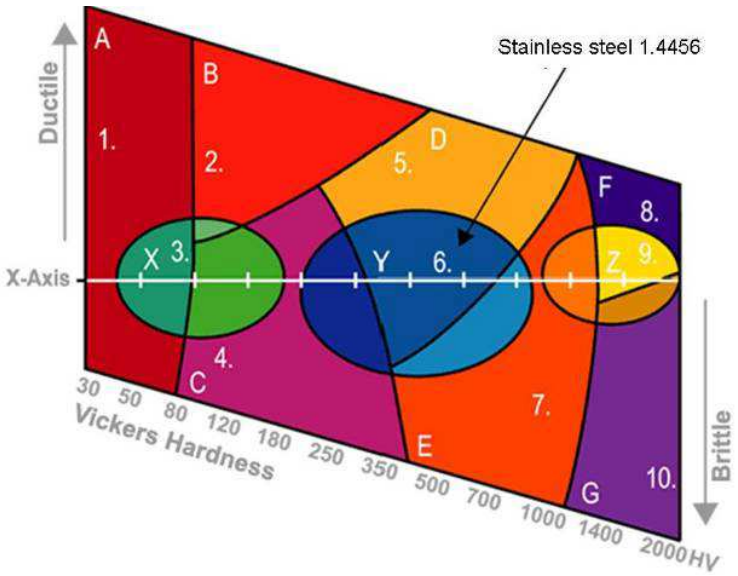

Fig. 2.1 Metalogram [4]

The preparation method depends on these mechanical properties. In the present work on thesis the austenitic stainless steels DIN 1.4456 fall into the category *tool steel* and therefore the **Metalog Method Y** (procedure 6). The aim of this procedure is to obtain a surface as much as possible reproducible.

The surface preparation is divided into two steps: grinding and polishing. A first step with abrasive silicon carbide paper with 500 mesh was performed to grind the surface and to ensure its planarity. Bidistillate water was used as cooling lubricant during the grinding and for removing abraded particles from the surface. This step allowed the removal of impurities, defects and the obtaining of a flat surface before the polishing. Fine grinding was carried out in successively finer steps using 1200-2400 meshes silicon carbide paper: each step lasted three minutes. Subsequently, the samples were dried using an argon stream. Fine grinding produces a surface with such a small amount of deformation that it can be removed during the polishing. A DP Plus cloth supplied by Struers with 3µm diamond past spray was used for the final **polishing**. This last step lasted five minutes; absolute ethanol was used as lubricant. The samples were dried using an argon stream at the end of the polishing.

2.2 Methods

2.2.1 Optical Microscopy

During the mechanical polishing of the sample surface after each step, the sample surface was examined using an optical microscope Zeiss Axiolab A. The microscope is equipped with a camera connected to a computer and it is possible to save the images taken at various magnifications. The surface of the steel samples was also examined following the color etching using an optical Microscope Zeiss FM Axioscope 2.

2.2.2 Contact angle goniometry

Static water contact angle were performed on a Krüss contact-angle measuring system (DSA-100, Krüss GmbH, Germany).

A drop of 8.5 µL was produced and then gently placed on the surface of the stainless steel. Thanks to a camera that allows having magnified images of the drop, it was possible to measure accurately the contact angle. An example of the image is shown in figure 2.2.

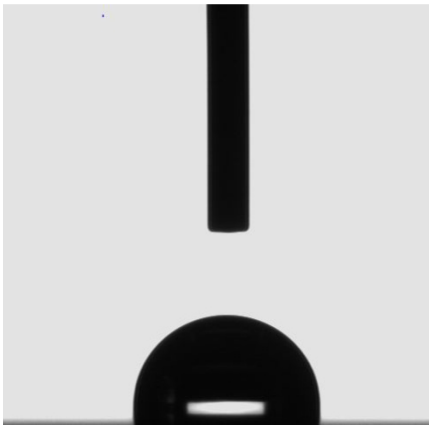

Fig. 2.2 Drop image to calculate static contact angle

The software used to static water contact angle measurement was the DSA3 and is used the *tangent method 2.* Three drops were created on each sample and contact angle was measured so that it was possible to calculate the standard deviation.

2.2.3 Electrochemical tests

The electrochemical tests were carried out using an electrochemical cell and a potentiostat connected to it. Two kinds of electrochemical cells have been used in this work: one is a cylinder of about 200 cm^3 volume, the other is a miniaturized one which allows using a smaller amount of the solution. This approach has been followed with the aim of measuring in the solution the amount of ions released by the steel in contact with the artificial saliva.

Electrochemical cell was a cylinder of plexiglass with a diameter of 8 cm and was provided with a lateral hole. The steel sample was fixed on it to improve the contact between solution and sample. The working surface area was 0.785 cm^2. To ensure a solution temperature of 37°C, inside the cell was inserted a spiral-hollow glass especially designed. The spiral was connected with tubes to a thermostat so that it was possible to set the desidered temperature. The cell was filled with an approximately 250 cm^3 of the artificial saliva in order to ensure the contact of the sample with the solution. The cell was closed with a lid with five holes for the insertion of the counter electrode, Luggin's capillary and reference electrode. The *working electrode* was the steel sample. It was always mechanically polished and then fixed with a copper plate on the cell wall before the electrochemical tests. The *reference electrode* was a saturated calomel electrode (SCE) and its potential versus hydrogen electrode is 241 mV at 25°C. This electrode was mounted into an

intermediate capillary filled with a saturated KCl solution and then inserted in a Luggin's capillary that was filled with a portion of the artificial saliva solution. The *counter electrode* used for these experiments was a platinum net.

Miniaturized electrochemical cell

This cell is composed of a steel disc on which is fixed the sample (working electrode). The cell is fitted with a plexiglass cylinder of diameter equal to 14 mm positioned above the sample. The cylinder is filled with the artificial saliva to ensure the contact with the sample . The cell is fixed with two screws and an o-ring in order to avoid the displacement of the steel and fluid leakage. The cell is a conventional cell with three electrodes: a calomel reference electrode was inserted in a capillary filled with a saturated solution of KCl; this capillary is then inserted in a Luggin capillary filled with the artificial saliva. The Luggin capillary has on the lower part (tip) of a twisted platinum wire (counter electrode). The OCP measurements were carried out by manually recording the potential after various immersion times in order to get more points. Fig. 2.2 shows its picture.

Figure 2.3 Miniaturized cell

The electrochemical experiments were carried out using a *Potentiostat-Galvanostat* by EG&G Model 273A. The software Softcorr Model 352 was used to record and save the measurements. The measurements performed in this investigation were: *open circuit potential, linear polarization, potentiodynamic polarization curves.*

- *Open circuit potential*

  The potential of the steel sample versus the reference electrode (SCE) was recorded upon the time of exposure to artificial saliva. In this work the tests were performed at increasing immersion times: 1-3-16-24-72 hours.

- *Linear Polarization*

  This experiment was used to obtain the polarization resistance by scanning the potential from ±20 mV around the OCP at the end of OCP test . The scan starts at -20 mV vs. OCP and ends at +20 mV vs. OCP. The current density (nA/cm^2) is measured vs. the applied potential (mV) and the plot results to be a curve characterized by a linear region. It was possible to determine Rp (polarization resistance) by calculating the slope of the linear region of the plot.

- *Potentiodynamic polarization curve*

In the following the procedure applied for obtaining the polarization curves is reported:

- The steel sample is placed in contact with the artificial saliva for 30 minutes in order to reach an OCP value stable within ± 20 mV;
- the cathodic and the anodic polarization curves were then recorded.

Between two acquisitions, the steel sample was again placed in contact with the saliva in order to restore the initial value of OCP. The parameters set for the data acquisition were: + 50 mV vs OCP to -1400 vs. OCP for cathodic scans and -50 vs. OCP to the transpassive potential for the anodic scans. Scan rate was 0.2 mV/s.

- *Data processing*

  The software used for data acquisition was 352 model Softcorr II mode ms-dos. The measurements were replicated at least twice and the data obtained were processed using Kaleidagraph (Version 4.0, Synergy Software).

2.3 X-ray Photoelectron Spectroscopy

The surface analysis was performed before and after exposure to the solution at the open circuit potential at 37° C for various time, using the Theta Probe (Thermo Fischer Scientific, East Grinstead, UK) spectrometer. A series of experiments were carried out at room temperature and sputtering depth-profiles were acquired using a Quantera SXM (ULVAC-PHI, Chanhassen, MN, USA).

2.3.1 Theta Probe

Theta Probe spectrometer is equipped with a monochromatic AlKα (1486.6 eV). In this work the source operated at 100 W, corresponding to 400 µm spot size in the constant-analyser-energy (CAE) mode. The instrument has two turbomolecular pumps, one operating in the fast entry lock chamber, the other in the analysis chamber. The pressure during experiments was always better than 10^{-9} mbar (10^{-7} Pa). It was also possible, thanks to the analyser / detector system, to register the spectra at 16 different emission angles ranging from 24.88 to 81.13 degrees in the so-called angle resolved mode (ARXPS). In standard mode the take-off angle was 53 degree. Three points have been selected on each sample in standard mode and one in angle resolved mode and the spectra were peak fitted using the parameters are listed in table 2.3, and are in agreement with other papers [5,6]. In standard mode the acquisition was performed using a pass-energy (PE) of 300 eV, and a step size 1.00 eV to record the survey spectra. High-resolution spectra were recorded with a pass-energy of 100 eV and step size of 0.100 eV. The acquisition in angle resolved mode was performed setting the pass-energy (PE) at 300 eV, the step size at 1.00 eV for the acquisition of the survey spectra while the acquisition of the high-resolution ones has been performed selecting a PE of 150 eV and step size of 0.05.

Signal	Component	Binding Energy (eV)	G/L
$Fe2p_{3/2}$	Fe (0)	706.8 ± 0.1	GL(85)T(0.80
	Fe (II) oxide + FeO sat.	709.4 ± 0.1 714.8 ± 0.1	GL(30)
	Fe (III) oxide	710.8 ± 0.1	GL(30)
	Fe oxy-hydroxide	712.4 ± 0.1	GL(30)
$Cr2p_{3/2}$	Cr(0)	573.9 ± 0.1	GL(65)T(1)
	Cr(III) oxide	576.4 ± 0.1	GL(30)
	Cr (III) hydroxide	577.9 ± 0.1	GL(30)
$Mn2p_{3/2}$	Mn (0)	638.9 ± 0.1	GL(80)T(0.55)
	MnO	641.2 ± 0.1	GL(90)
	MnO_2	642.5 ± 0.1	GL(90)

Tab. 2.3 Fit parameters

All samples were analysed after mechanical polishing and after the OCP experiments. Table 2.4 shows the energy ranges used of the spectral regions collected.

	Energy range (eV)
Survey	0-1400
C1s	279-298
O1s	525-545
Cr2p	568-594
Fe2p	701-735
Mn2p	632-670
Mo3d	222-242

Tab. 2.4 Energy ranges used of the spectral regions

2.3.2 Quantera

Composition vs depth profiles were performed by Argon ion etching by means of a PHI Quantera SXM spectrometer (ULVAC-PHI, Chanhassen, MN, USA). This spectrometer is equipped with an AlKα monochromatic source whose beam size ranges from 5 to 200 µm. Figure 2.3 below shows the scheme of the source [7].

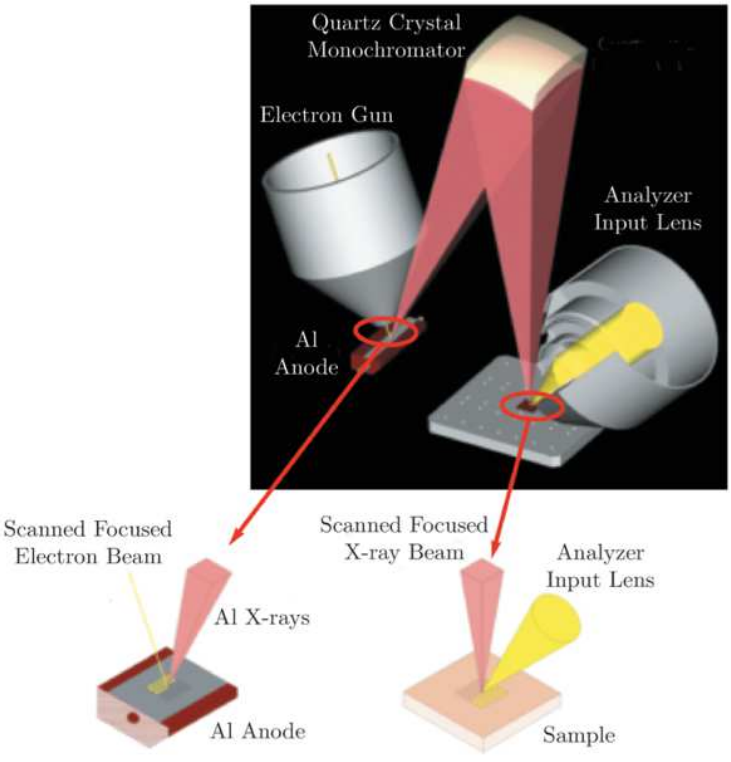

Fig. 2.3 Scheme of the AlKα source [5]

After electrochemical measurements carried out at room temperature, the samples were all analysed by sputtering depth profile. The experiment involved 10 cycles of sputtering of 30 sec. each; the first cycle was acquired without sputtering, so that the surface is representative of the sample without any further treatment. The survey spectra were acquired using a step size of 1.00 eV and a pass-energy (PE) of 280 eV while the high-resolution spectra were acquired setting the pass energy at 69 eV and with a step size of 0.125 eV. Table 2.5 shows the energy ranges used of the spectral regions collected.

	Energy range (eV)
Survey	-5-1400
C1s	279-299
O1s	526-546
Cr2p	568-608
Fe2p	701-741
Mn2p	633-673
Mo3d	224-244

Tab. 2.5 Energy range used of the spectral regions

2.3.3 Data processing

The spectra were processed using CASAXPS software (Version 2.3.16, Casa Software Ltd, Wilmslow, Cheshire, UK). In order to obtain the information on the different chemical states from the acquired spectra it was necessary to perform a procedure (curve fitting) that consisted of the background subtraction using the Shirley-Sherwood iterative method [8]. After background subtraction, the peaks were fitted using the Gaussian/Lorentzian functions determined on reference compounds measured under the same experiments conditions. A tail function has been added in order to account for a possible asymmetry of the peak. The area of the peak is directly proportional to the number of electrons ejected and from this it is possible to make quantitative analysis. The area of the signal, however, must be corrected for the parameters, which take account of instrumental factors and the nature of the material. In this work the first principles method [9] has been used; this approach is based on sensitivity factors calculated taking into account the contribution of the matrix and the instrumental parameters. Sensitivity factors are given by:

$$S = \sigma(h\upsilon) * L(\gamma) * T(E) * \Lambda$$

Where

□ = cross section of Scofield [10]

Λ = attenuation length

L(*γ*) = asymmetry factor [11]

T(E) = Transmission function also known as Intensity/energy response function

The transmission function of the PHI Quantera SXM spectrometer can be calculated as follows:

$$T(KE) = \left(\frac{a^2}{a^2 + RR^2}\right)^b$$

RR is the retard ratio, i.e. the ratio between the kinetic energy, KE, and the pass energy, PE. The parameters ***a*** and ***b*** can be calculated by fitting the intensity of Cu 2p3/2 divided by the pass energy versus the retard ratio.

The transmission function of the Theta Probe spectrometer is expressed by the following relation calculated by Thermo Fisher Scientific for the emission angle of 53°:

$$\log \frac{I}{E_p} = -0.0132(\log RR)^3 - 0.2519(\log RR)^2 + 0.3053 \log RR + 3.4253$$

The atomic percentage of the element is given by the intensity divided by the sensitivity factor:

$$\text{atomic } \% = \frac{I_i / s_i}{\sum_i I_i / s_i} \cdot 100$$

The composition of the surface film and of the film/alloy interface of the steel samples has been calculated using the three-layer model [12] that simultaneously allows the estimation of the thickness of the contamination and of the oxy-hydroxide layers.

This model assumes that the structure of nanometric films surface is formed by an outer layer with a thickness lc, an intermediate layer, such as an oxide or anoxy-hydroxide, and an inner layer which is the interface film / alloy. The model requires that the homogeneity of the layers and the absence of concentration gradients is fulfilled.

Another method for calculating the layer thickness by XPS used in this thesis was comparing the intensity of the signals at two different emission angles; the equation used to calculate the thickness is shown below,

$$\frac{I_m(\theta 1)}{I_m(\theta 2)} = exp\left[\frac{t^*}{\lambda_{ox}}\left(\frac{1}{cos\theta 2} - \frac{1}{cos\theta 1}\right)\right]$$

Where **t*** is the total thickness which also includes the contamination layer.

2.4 Analysis of solution after electrochemical tests by AES-ICP

Solution analysis was performed with an ICP Spectrometer iCAP 6000 series (Thermo Scientific) equipped with an ASX 260 autosampler (CETAC Technologies). The solutions from the microcells (each ca. 0.5 cm^3) were stored and later analysed for their chemical composition by ICP. The solution (or sometimes dry residues) was dissolved in 1 cm^3 of artificial saliva. 500 µL of each resulting solution was diluted to 25 cm^3 with HNO_3 2% (w/w) in ultrapure water.

References

[1] Tani, G. and F. Zucchi . Electrochemical measurement of the resistance to corrosion of some commonly used metals for dental prosthesis. Minerva Stomatol 1967. 16:710–713

[2] http://www.metallography.com/etching/table.htm (29-11-2013)

[3] http://mme.iitm.ac.in/gphani/lib/exe/fetch.php/om:vandervoort.pdf (29-11-2013)

[4] http://www.struers.com/default.asp?top_id=5&main_id=19&sub_id=25&doc_id=122

[5] B. Elsener, D. Addari, S. Coray, A. Rossi, Electrochimica Acta, Volume 56, Issue 12, 30 April 2011, 4489-4497

[6] S. Corey, Master thesis, High strength stainless steels for structural concrete–electrochemical and surface analytical investigation, 2009

[7] http://www.phi.com/surface-analysis-products/quantera/overview.html (29-11-2013)

[8] P. M. A. Sherwood in D. Briggs, M. P. Seah (eds.): Practical Surface Analysis, 1st ed. Vol.1, J. Wiley & Sons, Chichester 1983

[9] Seah M. P.: Quantification of AES and XPS, in Practical Surface Analysis, John Wiley & Sons (1990).

[10] Scofield J. H.: Hartree-Slater Subshell Photoionization Cross-Sections at 1254 and 1487ev. J. Electron. Spectrosc. 8, 129-137 (1976).

[11] Reilman R. F., Msezane A., and Manson S. T.: Relative Intensities in Photoelectron-Spectroscopy of Atoms and Molecules. J. Electron. Spectrosc. 8, 389-394 (1976).

[12] A. Rossi and B. Elsener, Surface and Interface Analysis, 18 (1992) 499 – 504

3 Results

3.1 Optical microscopy

All samples were polished following the instructions reported in the E-metalog by Struers and adapted to the present work as described in chapter 2, experimental. They were observed with a metallographic microscope. Metallographic preparation limits the presence of surface defects such as scratches, deformation, and impurities and allows obtaining of a surface as smooth as possible.

Figure 3.1 shows the images obtained with the optical microscope after grinding (3.1 a) and polishing (Fig. 3.1.b). The images show the changes in the surface finishing.

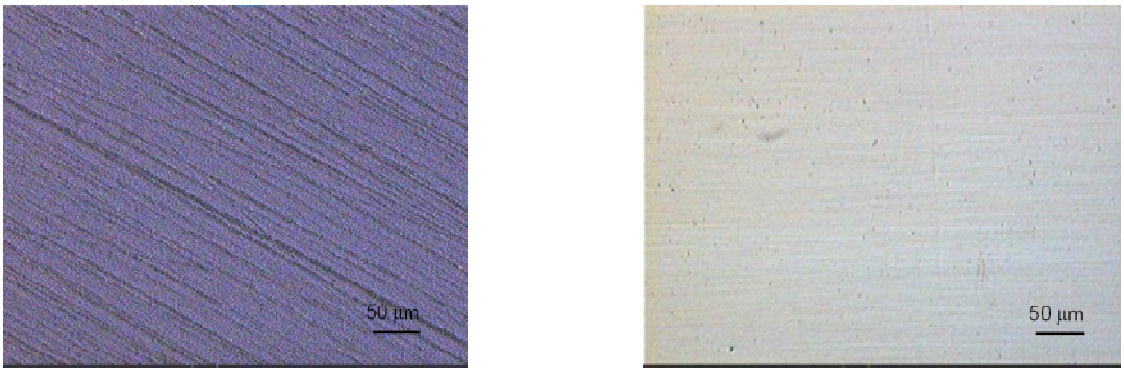

Fig. 3.2 Micrographs after 2400 mesh magnification 20x (left) and after polishing (right)

The micrograph on the left shows marked grooves after grinding with a SiC paper 2400 mesh while the subsequent elimination of scratches after the use of 3 µm diamond paste is apparent from the micrograph. This polishing procedure ensures that the sample surface has a very low roughness, the same morphology and surface composition.

Etching solution was used on samples of stainless steel to reveal the austenitic structure. The steel sample was immersed in a Beraha's solution (hydrochloric acid at 32% wt, potassium metabisulfite and distilled water). The steels disks were prepared as described above and then immersed in the solution for about 60-90 sec. and subsequently analysed by optical microscopy.

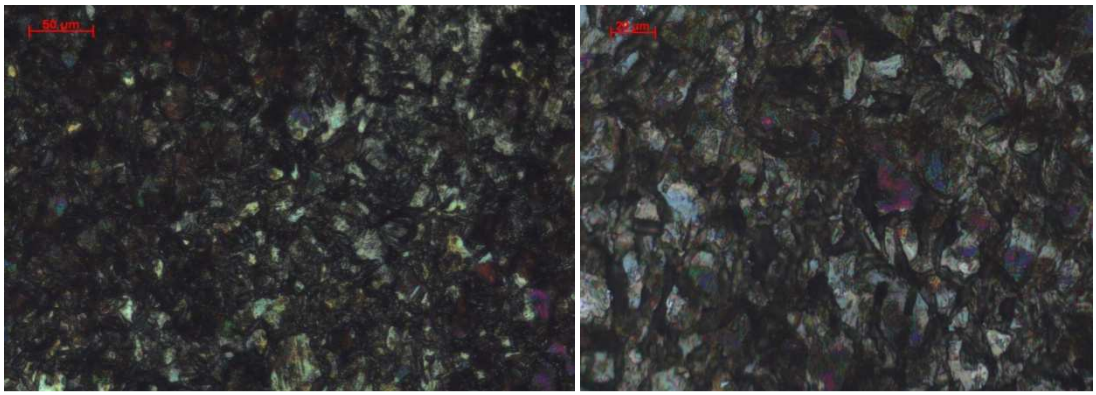

Fig. 3.3 DIN 1.4456 after color etching magnification 20x (left) and 40x (right)

Figure 2 shows the micrographs obtained after colour etching with a Beraha's solution.

Austenite is a solid solution of one or more elements in fcc (face centered cubic) iron. Using a tint etch that colours austenite, the grain structure can be revealed. The regular grain boundaries typical of the austenitic structure are clearly detected in the micrograph at the right.

3.2 Electrochemical results

3.2.1 Open Circuit Potential

The samples were mechanically polished with a 3 µm diamond paste, immersed in an ultrasonic bath for 5 minutes, dried with argon and then exposed to the artificial saliva solution.
All experiments were conducted at a temperature of 37 ° using a thermostating system through a system of tubes connected to the electrochemical cell. Electrochemical measurements were carried out for increasing immersion times in artificial saliva for 1 hour, 3 hour, 16 hour and 24 hour.

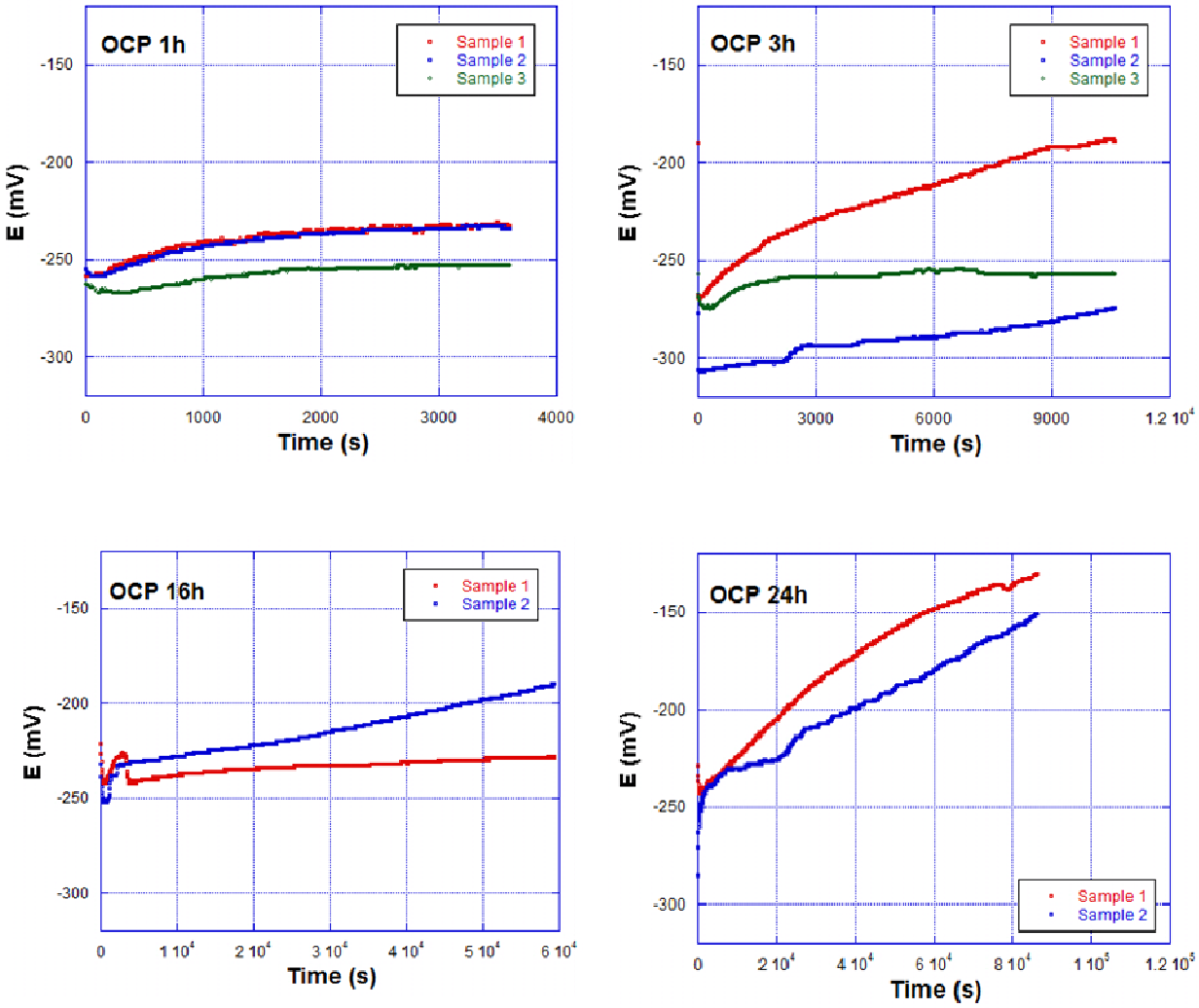

Figure 3.4 OCP vs time of the steel plate immersed in artificial saliva: 1-3-16-24 hours

The open circuit potential vs time plots obtained for different immersion times for the steel 1.4456 in artificial saliva are provided in figure 3.3. The curves show a similar trend. They start from negative initial potentials, around -250 mV vs SCE, and rise toward positive values, indicating the growth and the increasing stability of the passive film. The figure shows all measured OCP curves in artificial saliva. It can be seen that the initial value of all OCP measurements are similar.

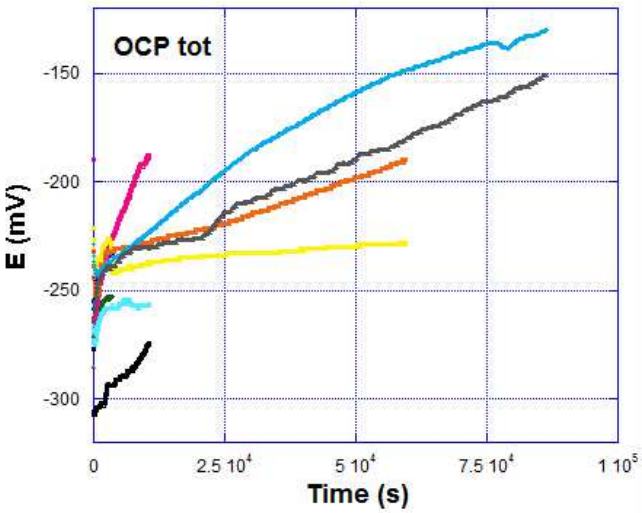

Figure 3.5 OCP Summary of all samples

Miniaturized cells

Open circuit potential measurements were also performed on the same samples at ambient temperature using microcells for 1 hour, 3 hours, 24 hours, 72 hours and 7 days. The open circuit potentials were measured manually for each sample.

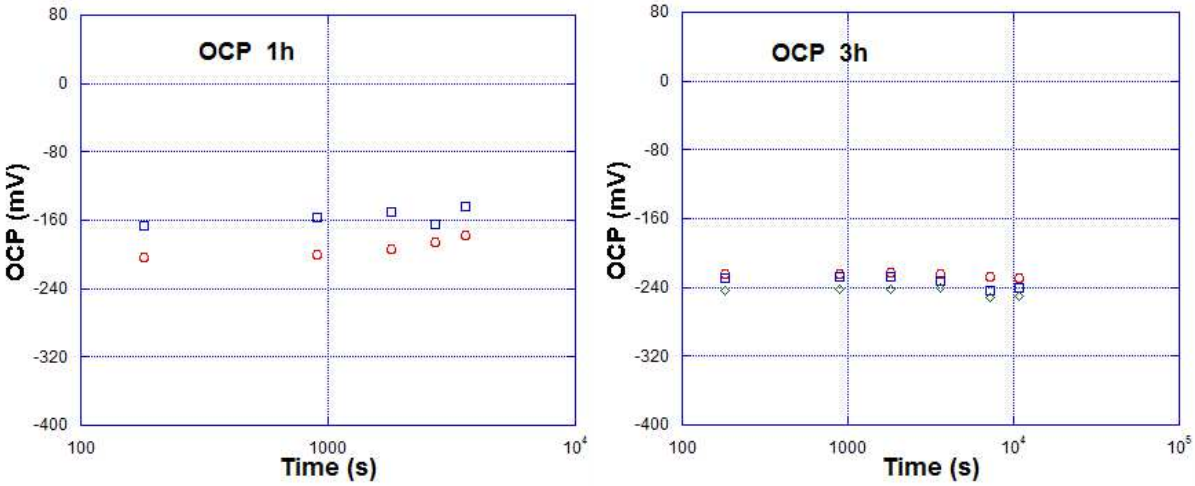

Figure 3.5 OCP vs time 1h and 3h

The OCP curves using the microcells (Figure 3.5) exhibit similar results compared to the OCP obtained at 37 ° C (Figures 3.4 and 3.5). The initial potential is also found at about -250 mV SCE and is also similar the evolution of the potential that starts from negative values, but it reaches more positive potentials upon time.

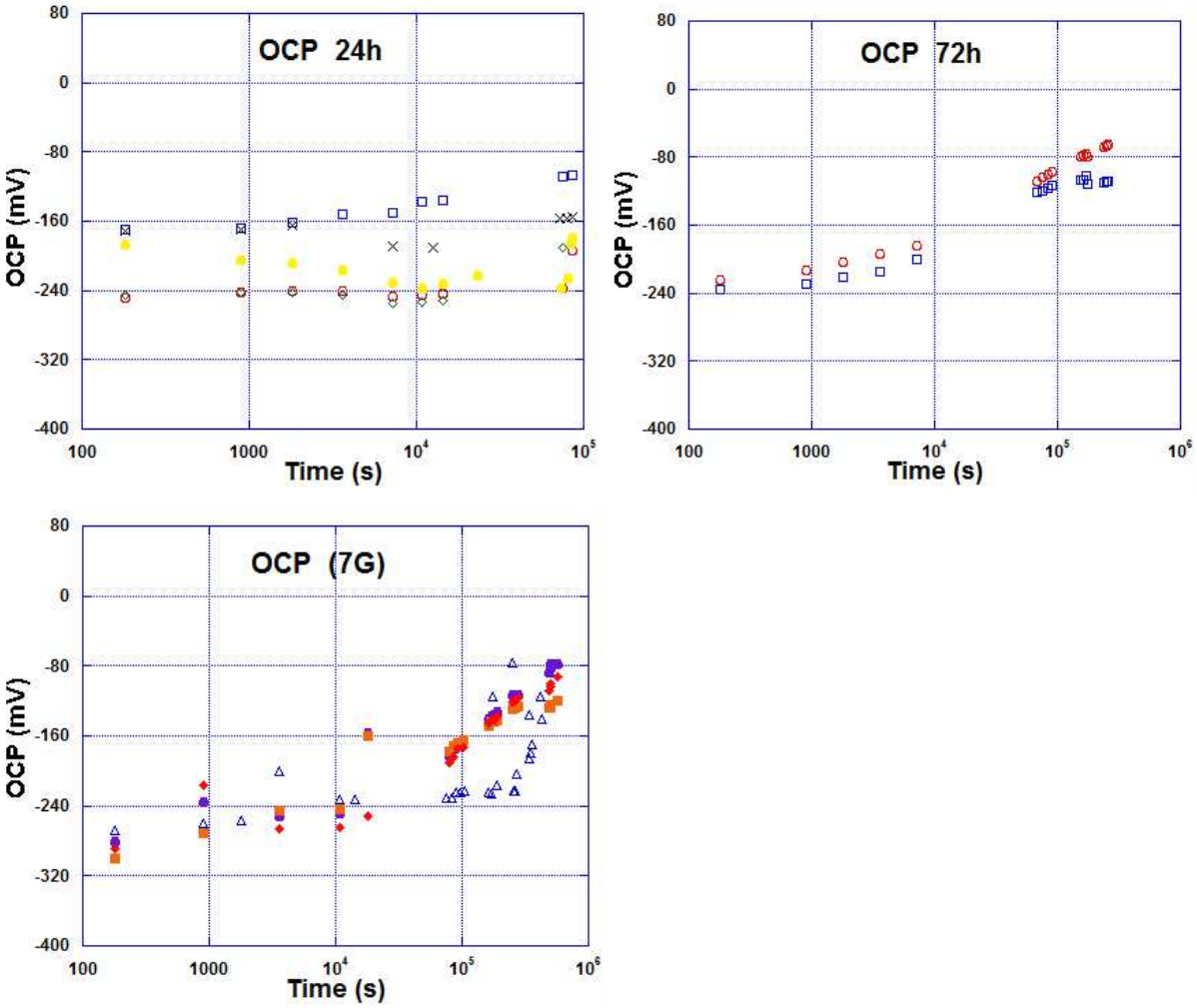

Figure 3.6 OCP vs time 24h, 72h and 7 days on microcells

3.2.2 Linear polarization

The linear polarization curves were recorded by scanning the potential range from -20 mV to +20 mV versus OCP. The recording of the polarization resistance has been carried out on the samples immediately after the finishing of the OCP measurements. The figure 3.7 show the linear polarization curves of all samples. As can be observed, a shift of the curves of the steel occur (more pronounced after 3 and 24 hours) which derives from the final OCP. From the slope of the curve, the corrosion density of the samples in artificial saliva can be calculated using the constant B of 52 mV for steels in passive state. The obtained values are in a range from 0.3 to 0.02 $\mu A/cm^2$ and are reported in the tab. 3.1 with Rp, OCP and vcorr values.

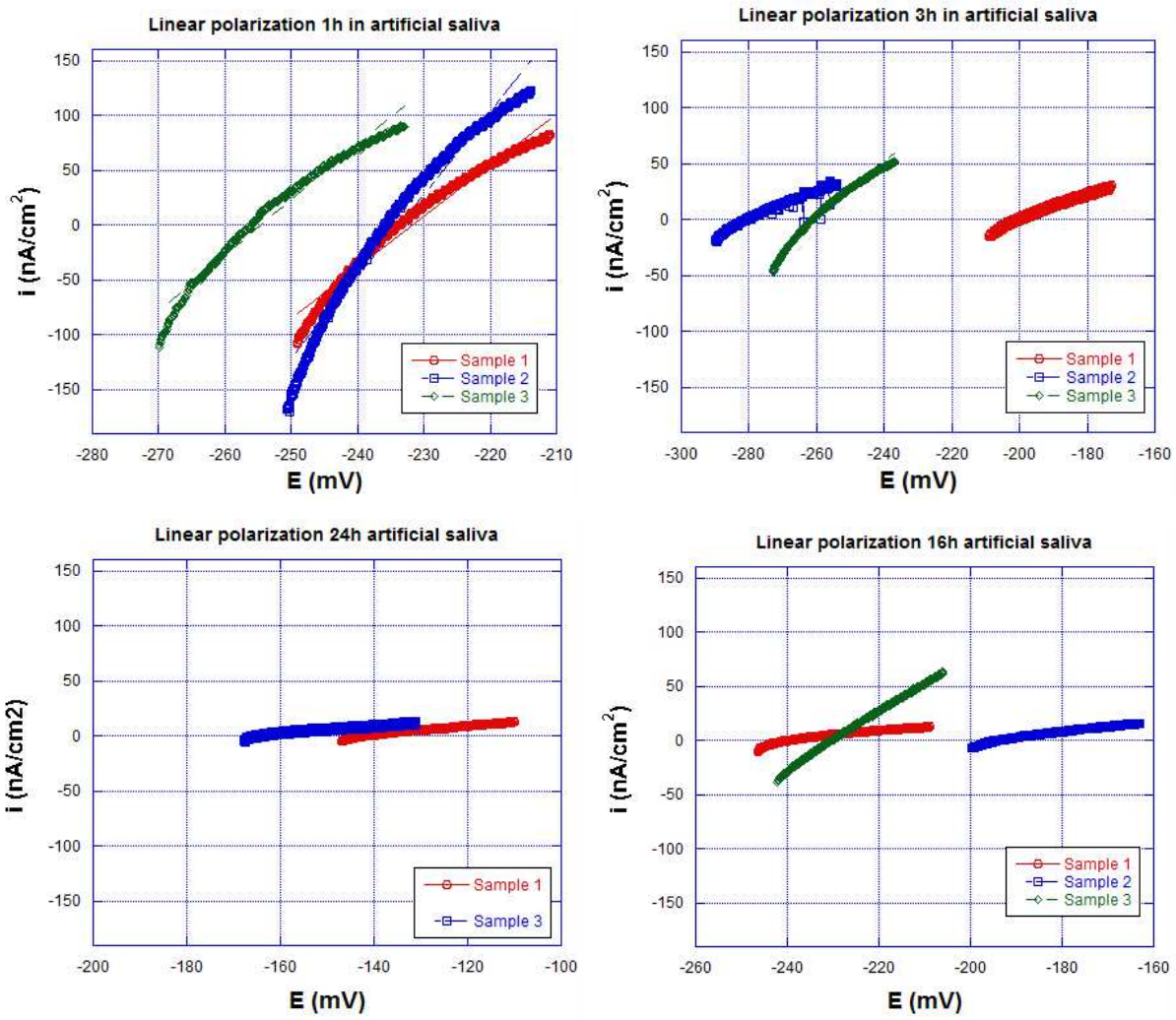

Figure 3.7 Linear polarization DIN 1.4456 in artificial saliva: 1-3-16-24 hours

Tab. 3.3 OCP, Rp, icorr, vcorr values of all samples immersed in artificial saliva

Time (h)	OCP (±20mV)	R_p(MΩ*cm^2)	i_{corr} (µA/cm^2)	Vcorr (µm/year)
1h	-258	0.21	0.24	2.82
1h	-255	0.13	0.39	4.54
1h	-262	0.20	0.26	3.01
3h	-268	0.87	0.06	0.70
3h	-306	0.77	0.07	0.78
3h	-267	0.39	0.13	1.55
16h	-221	2.09	0.03	0.29
16h	-232	1.81	0.03	0.31
16h		0.37	0.14	1.63
24h	-229	2.40	0.02	0.26
24h	-285	2.92	0.02	0.21

Tab. 3.4 Average of the values of Rp, icorr and vcorr

Time (h)	R_p(MΩ*cm^2)	i_{corr} (µA/cm^2)	Vcorr (µm/year)
1h	0.18±0.04	0.30±0.07	3.45
3h	0.68±0.25	0.09±0.04	1.01
16h	1.42±0.90	0.07±0.06	0.74
24h	2.67±0.40	0.020±0.006	0.23

As can be observed in Table 3.1 and 3.2 (average of the values) the values of i_{corr} decrease with immersion time. In the first hour of contact the i_{corr} value is ca. 0.3 µA/cm^2. The passive film is forming but it is still too thin. As the immersion time increases, the passive film becomes more stable justifying a decrease of i_{corr}. The i_{corr} value after 24 hours of contact amounts at 0.02 µA/cm^2 , a typical value for steel in the passive state. This trend can be observed more clearly in the summary plot in figure 3.8.

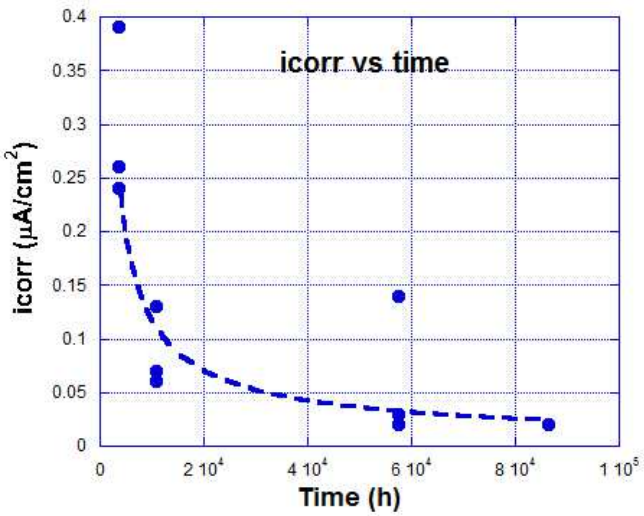

Figure 3.8 Summary plot of the variation of icorr vs. time

Based on the average corrosion rate (table 3.2) an attempt was made to calculate the mass loss over the time of immersion for samples exposed to artificial saliva at 25°C for several days (see chapter 3.3.2). Assuming a steady state corrosion rate of 0.1 µm/year, one can calculate the mass loss for the different immersion times with $\Delta m = 0.1\mu m/year * t_{immersion} / 352$. The results given in table 3.3 might be on the very upper limit because the dissolution rate at very long immersion times might be even lower then 0.1 µm/year (see figure 3.5).

Tab. 3.5 Calculation of the weight loss from icorr

Time	weight loss (µg)
1 h	0.02
3 h	0.28
16 h	1.72
24 h	1.88
3d	2.47
7d	3.10

The solutions of the micro-cells were analysed with ICP (see chapter 3. 5).

3.2.3 Potentiodynamic polarization

The anodic and cathodic polarization curves of steel 1.4456 in artificial saliva were recorded; figure 3.9 illustrates the behaviour of two samples of the alloy. The curves were recorded after being at OCP for 30 minutes with a scan rate of 0.2 mV/s; the solution was stirred constantly and in contact with air.

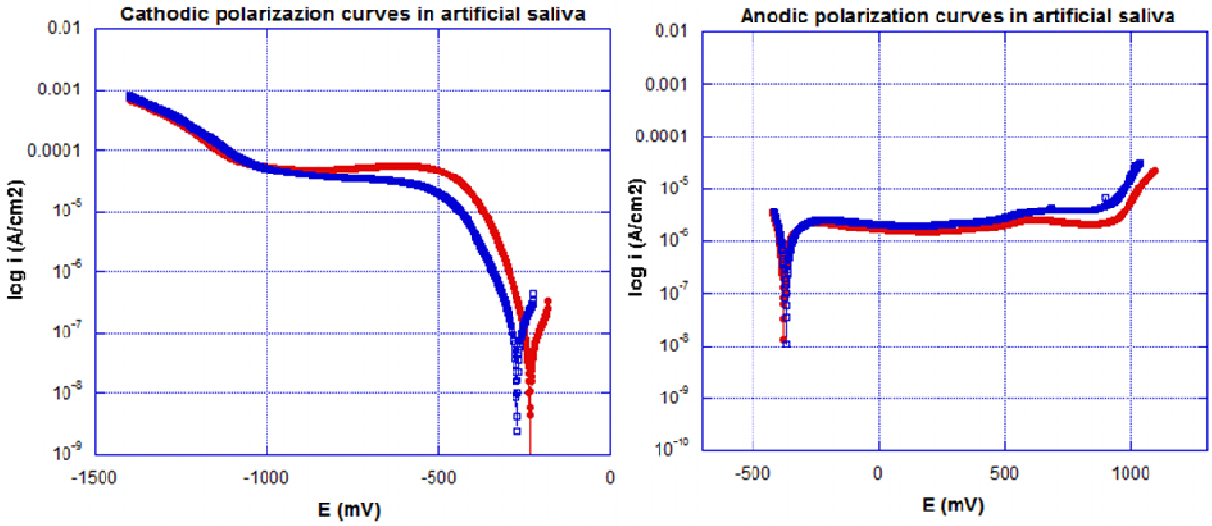

Figure 3.9 Cathodic and anodic and polarization curves of DIN 1.4456 in artificial saliva

The cathodic curves show low cathodic current densities of $2*10^{-5}$ to $4*10^{-5}$ A/cm^2. Within the analysed range of potential from +50 mV OCP to -1400 mV SCE can be observed a plateau range starting from -500 mV to -850 mV due to diffusion limited oxygen reduction. This limiting current observed is due to the slow transport of oxygen in the solution and depends on the oxygen availability on the metal surface. The current density increases exponentially again at more negative potential from -850 to -1400 mV when hydrogen evolution starts.

The anodic curve shows a typical behaviour of a steel in the passive state. The anodic scan started 75 minutes after the end of the cathodic scan in order to allow to recover the initial open circuit potential. The anodic polarization curves show a potential range (-200 to +600 mV SCE) where the current density is constant. At ca. +600 mV a current density increase occurs, due to the transpassive dissolution of chromium (III) to chromium (VI). As can be observed, at higher potentials over +600 mV SCE the current density starts to increase quickly due to the evolution of oxygen.

3.3 XPS results

In this section the results of the X-ray photoelectron spectroscopy are illustrated. In the first paragraph the XPS results of the surface films formed on DIN 1.4456 steel after mechanical polishing are described. The following paragraphs will present the results obtained after exposure of the samples to the artificial saliva at the temperature of 25 °C using microcells and at temperature of 37 °C. The composition of the passive film as well as of the interface beneath the passive film, together with its thickness allow the investigation of both the effect of exposure time and of the temperature on the formation of the film.

3.3.1 Mechanically polished samples

All samples were always mechanically polished using the protocol described in section 3.1 before exposing the sample surface to artificial saliva. Each sample was characterized by XPS. A survey scan was first acquired in order to identify the elements present at the surface of the alloy. After an accurate calibration of the spectrometer it is possible to identify the peaks related to the elements present.

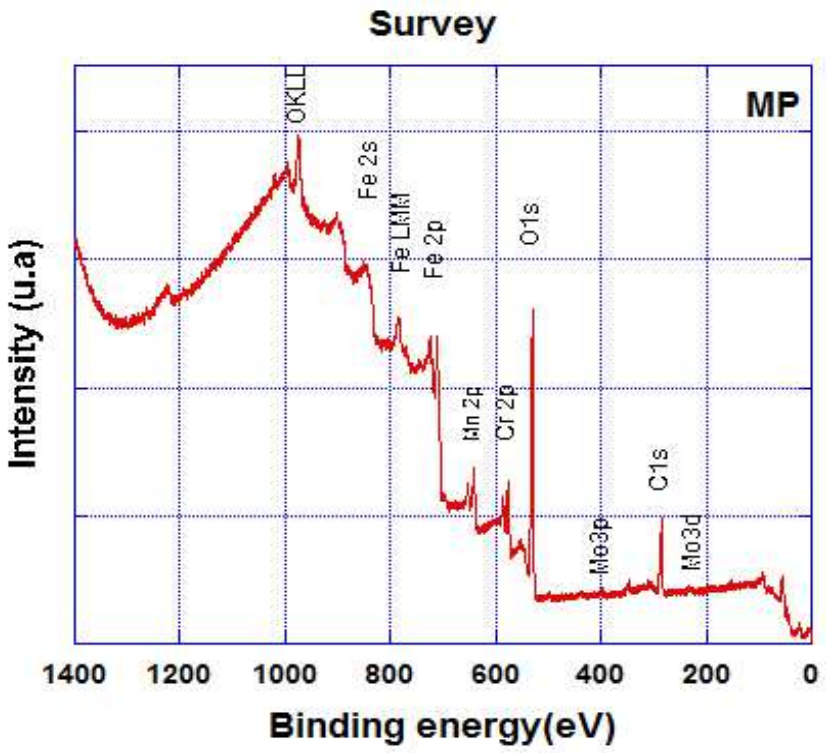

Figure 3.10 Survey scan of the mechanically polished DIN 1.4456

Figure 3.10 shows the survey scan of the sample after mechanical polishing. The elements present in the alloy visible in the survey spectrum are iron, manganese, chromium and molybdenum (not clearly visible). There are also the peaks relative to oxygen, due to the oxidation of the surface of the sample and carbon, due to contamination. The high-resolution spectra of C1s, O1s, Fe2p, Cr2p, Mn2p and Mo3d were acquired and processed. Figure 3.11 shows the spectra after mechanical polishing. The high-resolution spectra are processed after background subtraction. The binding energies of the components obtained by curve-fitting the signals with model curves are in agreement with the previous works of our group [1,2,3] and are presented as follows :

1. The signal relative to C1s originates from a contamination layer on the sample surface. This signal consists of three components, aliphatic hydrocarbon (most intense) at 285.6±0.1 eV and other two components relative to C-OH group at 287.3± 0.1 eV and COO group at 289.5±0.1 eV.
2. The oxygen O1s spectra present three contributions: at 530.2± 0.1 eV the oxygen in oxides as Cr, Fe and Mn oxides; the second component at 532.0±0.1 eV is ascribed to oxygen in hydroxide and the third component at 533.8±0.1 eV to adsorbed water.
3. The Cr2p signal consists of three components: metallic chromium (573.9±0.1 eV), chromium (III) oxide at 576.4±0.1 eV and chromium (III) hydroxide at 578.0±0.1 eV.
4. The Fe 2p signal presents four components: the first one, most intense, assigned to metallic iron at 706.8±0.1eV while the components of the oxidized iron are respectively: Fe (II) at 709.4±0.1 eV with its satellite at 714.7±0.1 eV, Fe (III) oxide at 710.8±0.1 eV and the oxy-hydroxide component at 712.4±0.1 eV.
5. The manganese Mn2p spectra contains four contributions: the first one is the metal manganese at 638.7±0.1 eV, manganese (II) oxide at 640.9±0.1 eV and the last one is manganese (IV) oxide at 642.5±0.1 eV.
6. Molybdenum 3d peak is very complex due to the low signal-to-noise ratio and the superposition of two contributions of the spin-orbit doublet ($3d_{5/2}$ and $3d_{3/2}$)). The metallic component was found at 227.5±0.1 eV and from molybdenum in oxidized state mainly Mo(VI) oxy-hydroxides at 230.6±0.1 and 232.3±0.1 eV.

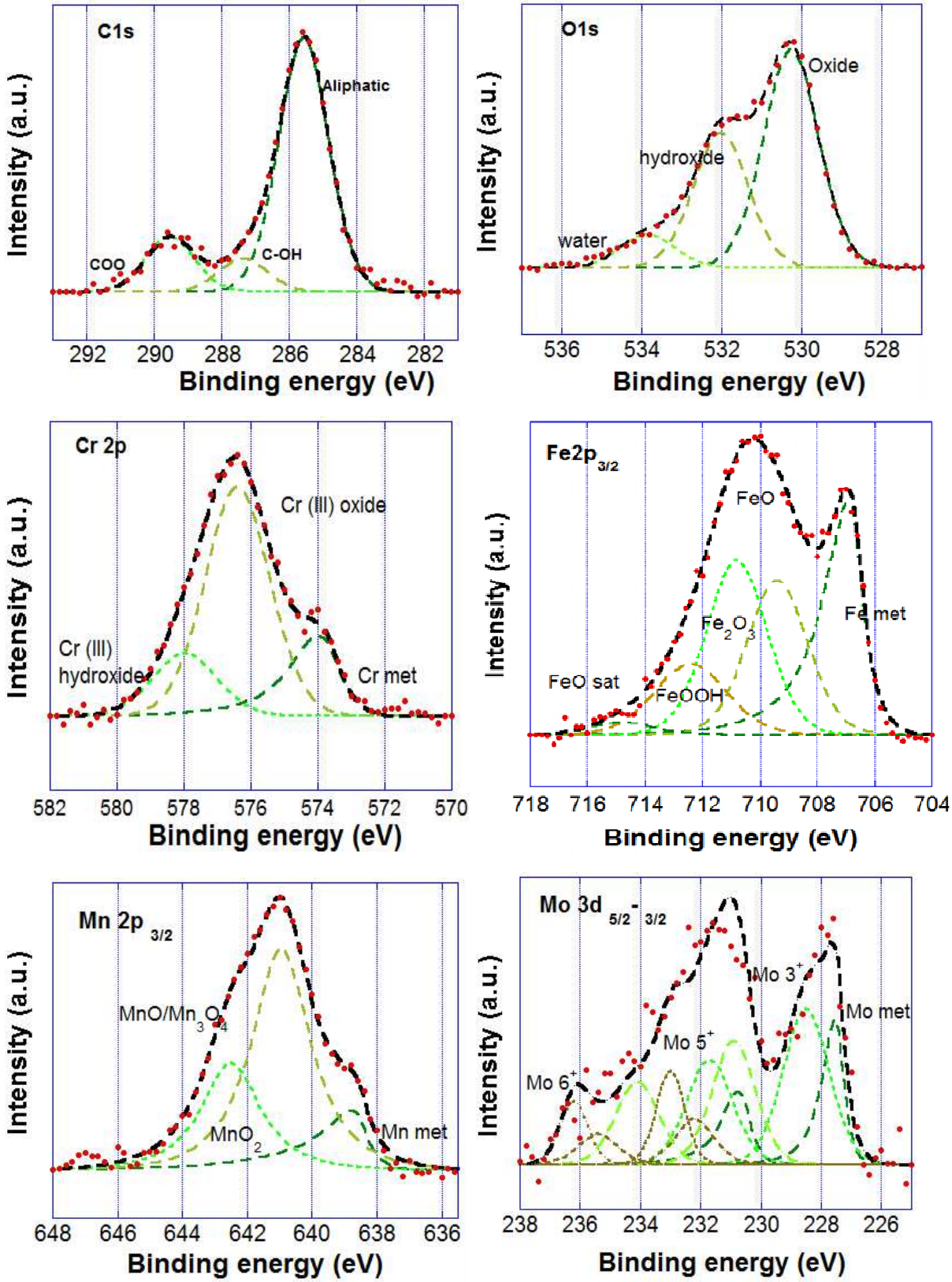

Figure 3.11 High-resolution spectra after curve fitting for the mechanically polished DIN 1.4456

3.3.2 Passive film formed at the OCP at 25°C

The samples have been exposed to artificial saliva for 1 hour, 3 hours, 24 hours, 72 hours and 7 days (168h) using the microcells (chapter 3.2.1) in order to evaluate the effect of ageing on the surface film. The different immersion time causes changes in the passive film.

Film thickness

The film thickness upon immersion time, tends to decrease compared to mechanically polished surface state, up to 3 hours and then increases at longer exposure times (see figure 3.12 and table 3.4)

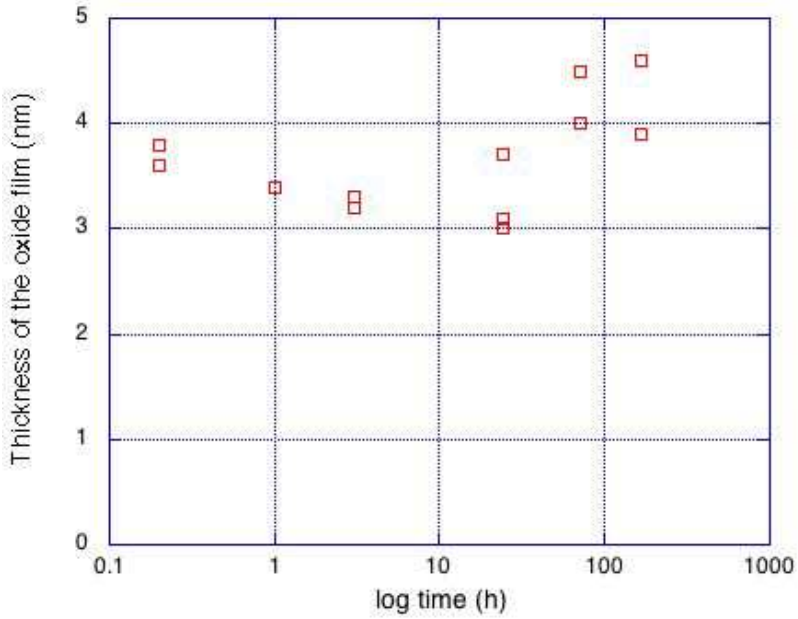

Figure 3.12: Average film thickness of the oxide film on alloy DIN 1.4456 exposed to artificial saliva (25°C)

Oxide film composition

The surface composition of the samples immersed in artificial saliva at 25°C was calculated with the three-layer model [4]. The resulting cation content of the passive film is reported in table 3.4. The table shows that the content of chromium oxy/hydroxide in the film is progressively increasing with the immersion time while the manganese content decreases compared to the nominal composition. An enrichment of molybdenum content is clearly detected.

Table 3.4: Thickness and composition (accuracy estimated to be not lower than 10%) of the oxide film formed on alloy DIN 1.4456 exposed to artificial saliva (25°C)

Time (h)	Thickness nm (±0.1nm)	Fe ox weight%	Mn ox weight%	Cr ox weight%	Mo ox weight%
MP	3.6	52.4	18.6	24.9	4.0
MP	3.8	54.5	18.4	23.7	3.4
MP	3.8	48.5	16.8	30.6	4.1
1	3.4	53.8	10.7	33.2	3.4
1	3.4	52.3	9.7	33.2	3.7
3	3.2	60.8	11.8	24.1	2.3
3	3.3	58.7	11.3	26.6	3.2
3	3.3	62.8	9.7	24.4	3.0
24	3.0	59.0	12.8	24.8	3.6
24	3.7	56.1	15.3	25.0	3.7
24	3.1	55.6	13.6	27.5	3.3
72	4.0	56.0	15.7	25.8	2.6
72	4.5	42.8	14.8	38.9	3.9
168	3.9	47.7	18.1	30.2	4.2
168	4.6	44.6	18.0	32.6	2.6
Average		**53.7±5.8**	**13.0±4.9**	**28.3±4.5**	**3.4±0.6**

Composition of the alloy beneath the oxide film (interface)

The composition of the alloy beneath the oxide film formed after immersion in artificial saliva at 25°C was calculated with the three-layer model. The resulting alloy composition is reported in table 3.5. The table shows that the content of chromium and molybdenum at the interface correspond approximately to the bulk composition (slight enrichment), manganese instead is strongly depleted. There are no significant variations with exposure time.

Table 3.5: Composition of the alloy beneath the oxide film after exposure to artificial saliva (25°C)

Time (h)	Fe met	Mn met	Cr met	Mo met
MP	70.6	4.7	22.0	2.7
MP	73.9	4.2	18.2	3.6
MP	72.6	5.5	19.5	2.3
1	70.0	6.4	20.6	3.0
1	70.0	8.1	20.0	2.0
3	68.0	12.5	17.2	2.3
3	66.0	7.8	23.7	2.6
3	66.4	7.3	23.6	3.2
24	66.5	10.6	21.0	1.9
24	61.9			3.7
72	71.5			3.4
72	62.5		22.3	3.9
168	64.1	9.0	24.1	2.8
168	48.2	2.9	46.6	2.3
168	48.6	0	46.1	5.3
Average	**65.4±7.7**	**6.6±3.4**	**25.0±9.7**	**3.0±0.9**

Composition of the surface film after 30 seconds of sputtering with argon ions

After 30 seconds of sputtering with argon ions the contamination layer and most of the oxide film has been removed. The residual oxide thickness is in the range from 0.2 to 0.4 nm (except one sample at 72 h). The three-layer model was used to calculate the average composition of the thin residual oxide film still present on the surface. A marked enrichment in manganese oxide and less pronounced in chromium and molybdenum oxide can be noted. Iron oxide is strongly depleted, indicating that in the inner part of the oxide film, iron oxide is present in lower amounts.

Table 3.6: Thickness and composition of the residual oxide film present on alloy DIN 1.4456 after exposure to artificial saliva and 30 seconds of sputtering with argon ions (25°C)

Time (h)	Thickness nm	Fe ox	Mn ox	Cr ox	Mo ox
MP	0.3	29.6	38.4	24.2	7.8
MP	0.3	20.3	41.8	29.5	8.3
MP	0.3	23.9	41.6	28.7	5.6
1	0.2	37.0	33.6	25.4	4.0
1	0.2	24.0	40.2	21.4	
3	0.2	28.7	33.5	30.3	7.5
3	0.2	29.1	40.0	24.8	5.9
3	0.2	25.7	38.8	31.2	4.2
24	0.1	38.7	26.7	17.4	5.1
24	0.2	28.4	32.5	29.1	2.9
24	0.2	33.1	30.6	19.8	6.6
72	0.4	24.8	33.9	30.5	6.5
72	1.6	17.6	32.5	44.9	2.6
72	0.6	33.8	15.4	30.4	3.1
168	0.3	29.0	32.8	27.3	4.0
168	0.3	22.6	27.6	26.7	9.5
168	0.5	22.6	32.1	28.0	4.5
Average	**0.4±0.3**	**27.6±5.8**	**33.6±6.6**	**27.6±6.0**	**5.5±2.1**

Composition of alloy beneath the film after 30 seconds of sputtering with argon ions

After 30 seconds of sputtering with argon ions the contamination layer and most of the oxide film have been removed. The residual oxide thickness is in the range from 0.2 to 0.4 nm (except one sample after exposure for 72 h). The three-layer model was used to calculate the average composition of the alloy beneath the oxide film. A marked depletion in metallic manganese and enrichment in molybdenum can be noted. Combining the information of film thickness (table 3.6) and metallic manganese (table 3.7) it can be noted that the concentration of manganese at the interface decreases with the residual film thickness (figure 3.13).

Table 3.7: Composition of the alloy beneath the oxide film after exposure to artificial saliva (25°C) and sputtering for 30 seconds

Time (h)	Fe met	Mn met	Cr met	Mo met
MP	71.8	5.6	18.1	4.6
MP	72.3	6.2	17.2	4.3
1	68.7	8.3	18.5	4.4
1	68.5	8.1	19.1	4.3
3	70.2	8.3	17.1	4.4
3	70.2	8.3	17.1	4.4
24	72.1	7.3	17.7	2.9
24	71.1	7.1	17.4	4.4
72	72.4	5.3	18.1	4.2
72	76.1	1.7	17.7	4.4
72	73.1	4.8	18.0	4.1
168	71.5	5.9	20.1	4.0
168	71.9	5.1	19.9	4.1
Average	**71.1 ±1.9**	**6.3±1.9**	**18.2 ± 1.0**	**4.3 ± 0.4**

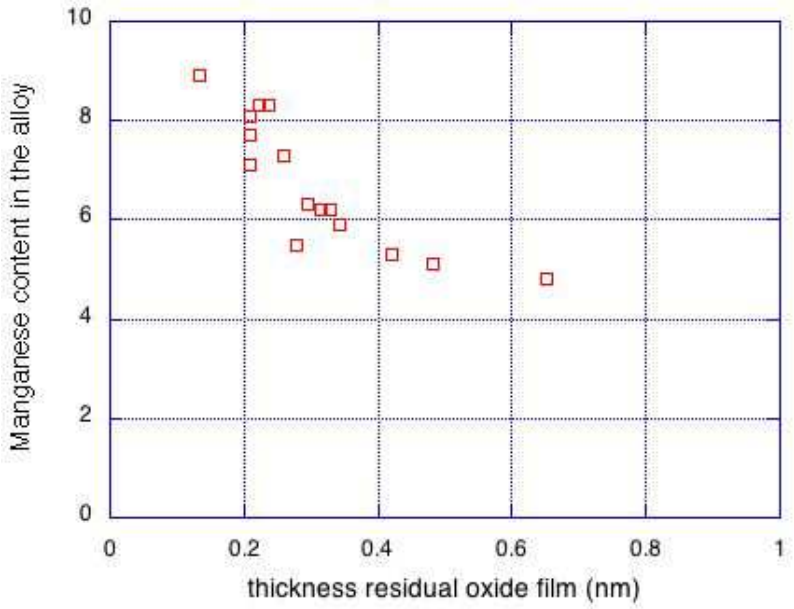

Figure 3.13: Average film thickness of the oxide film on alloy DIN 1.4456 exposed to artificial saliva (25°C)

Bulk alloy composition

The surface composition of the alloy after 10 cycles of argon ion sputtering of 30 seconds each is listed in table 3.8 as weight percentage. First of all, the bulk composition determined by XPS on 17 different samples shows perfect reproducibility. Moreover, molybdenum is strongly enriched (6.8%) respect to the nominal composition (1.9%). Chromium is slightly enriched (22% instead of 17.9%) while the manganese content is strongly depleted (11.5%) with respect to the nominal composition (18.4%).

Tab. 3.8 Bulk composition after 300 sec of sputtering with argon ions

Bulk composition (weight %)				
Time (h)	Fe	Mn	Cr	Mo
MP	60.0	12.2	21.4	6.4
MP	57.1	12.4	23.3	7.1
MP	59.7	11.4	22.0	6.8
1	58.7	11.9	22.6	6.8
1	60.0	11.5	22.6	6.0
3	59.3	11.5	22.6	6.5
3	59.8	11.1	22.3	6.8
3	59.6	11.5	22.1	6.8
24	58.9	11.4	22.8	6.8
24	59.2	11.7	22.6	6.5
24	60.3	11.4	21.5	6.8
72	59.4	11.8	22.1	6.7
72	59.3	11.9	21.8	6.9
72	59.2	11.9	22.0	6.9
168	59.0	11.5	22.6	6.9
168	59.1	11.4	22.7	6.8
168	59.2	11.4	22.6	6.8
Average	**59.3±0.7**	**11.6±0.3**	**22.3±0.5**	**6.7±0.3**

3.3.3 Passive film formed at the OCP at 37°C

Survey spectrum

The survey scan of the alloy after immersion for 24 hours in artificial saliva is provided in figure 3.14. The survey spectrum shows the peaks of the alloy (Fe, Cr, Mn, Mo), of carbon, C1s, and oxygen, O1s. The intensity of the carbon signal is usually higher than in the case of mechanically polished samples. High-resolution spectra after immersion of 24 hours do not show relevant changes in the binding energies of the component peaks with respect to the mechanically polished alloy (fig.3.14).

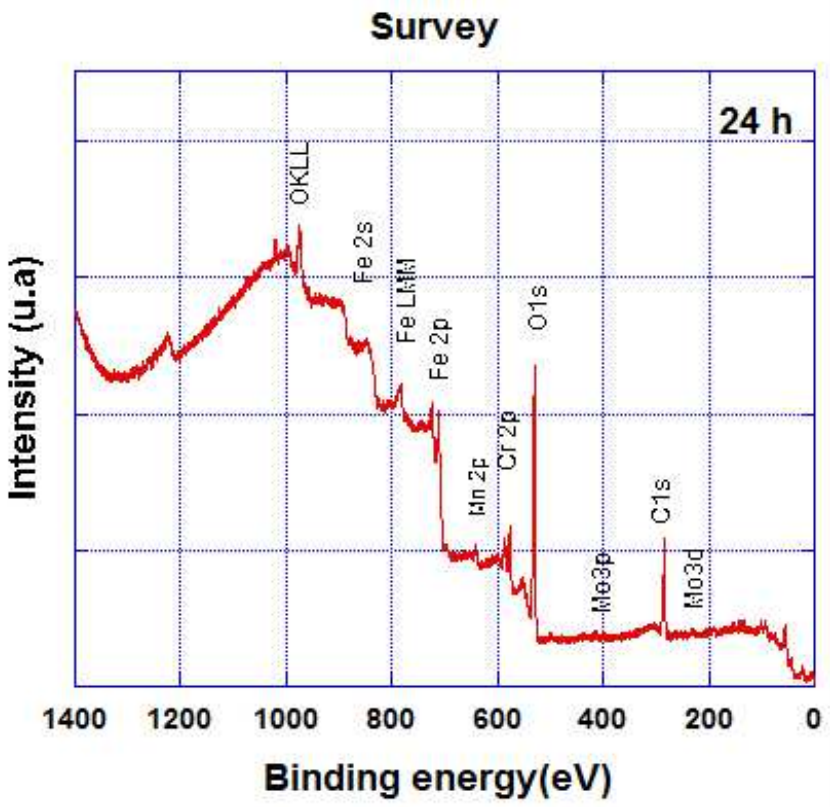

Fig. 3.14 Survey scan of stainless steel DIN 1.4456 after 24 h in artificial saliva (37°C)

High-resolution spectra

The high-resolution spectra of Fe2p, Cr2p and Mn2p of the alloy after immersion for 24 hours in artificial saliva are shown in figure 3.15. Compared to the mechanically polished alloy no significant changes in the binding energy of the different compounds present is observed. The contribution of iron (II) oxide (FeO) decreases whereas the iron (III) oxide increases.

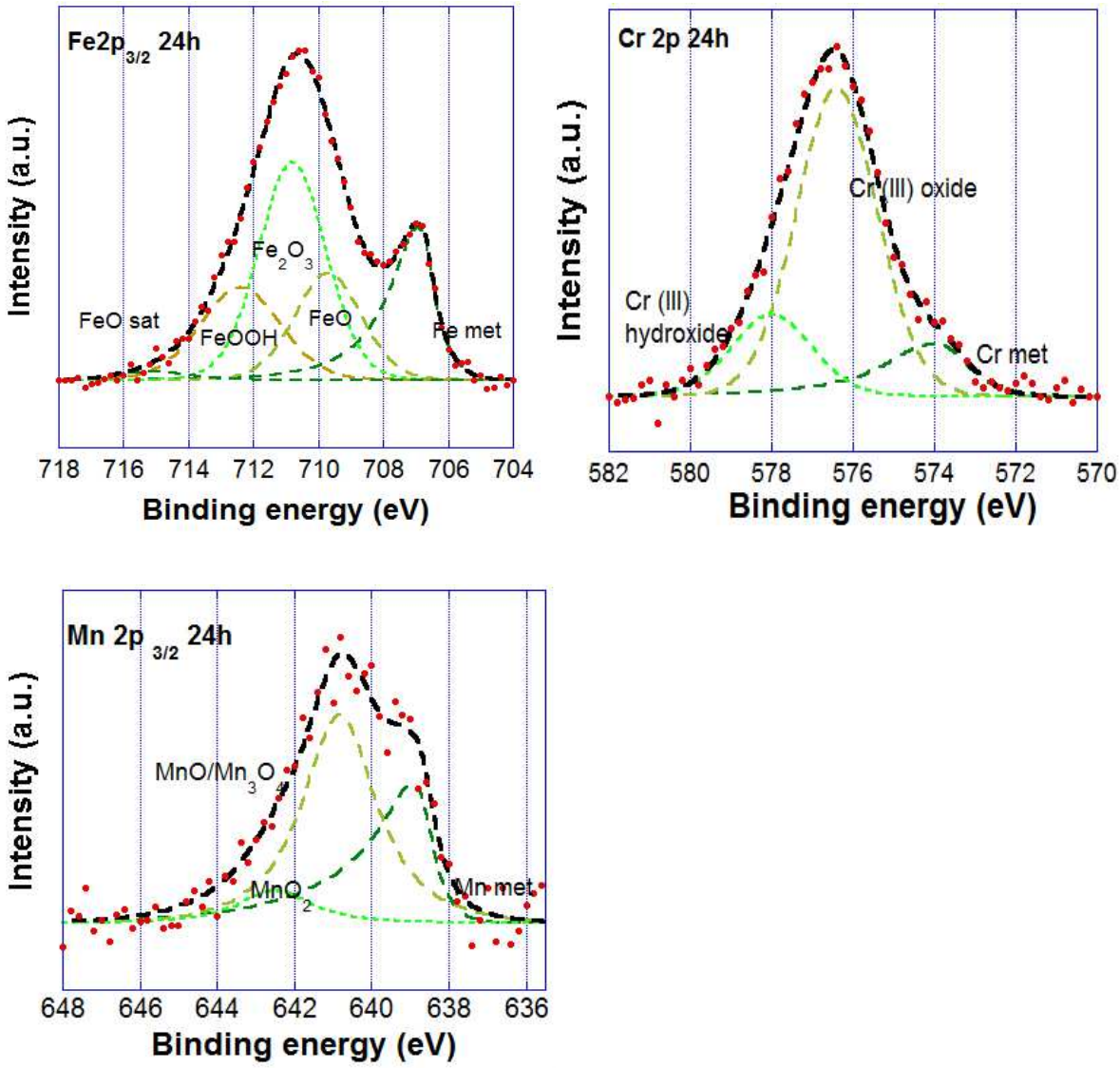

Fig. 3.15 High-resolution spectra of Fe2p, Cr2p and-Mn2p of the alloy DIN 1.4456 after 24 h in artificial saliva (37°C)

Angle resolved XPS

Angle-resolved XPS spectroscopy using the Thetaprobe spectrometer was performed on all samples. The spectrometer acquires data in the range from 24.8 to 69.8 degrees emission angle without tilting the sample thus ensuring that the spectra were all obtained from the same analysis point. The high-resolution spectra of Fe2p, Cr2p and Mn2p and the carbon contamination C1s were used to calculate thickness and composition of the contamination layer, of the oxide layer and of the metallic interface for all angles. This allows the identification of the oxide components present more at the outer or at the inner layer of the surface film. The composition calculated for each sample at the different angles is given in the Appendix II.

Mechanically polished samples

The composition of the oxide film for the mechanically polished samples is presented in figure 3.16. The composition of the oxide film is homogeneous at all analysed angles, comprised of 50% iron oxide, 35% chromium oxide and 15% manganese oxide. The composition of the alloy beneath the oxide film is given in table 3.9.

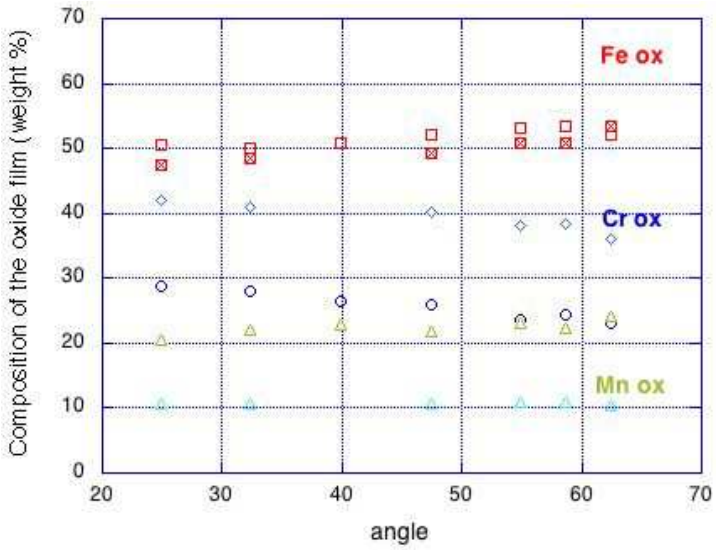

Fig. 3.16 Composition of the oxide film for mechanically polished 1.4456 samples

Samples exposed for 1 h to the artificial saliva

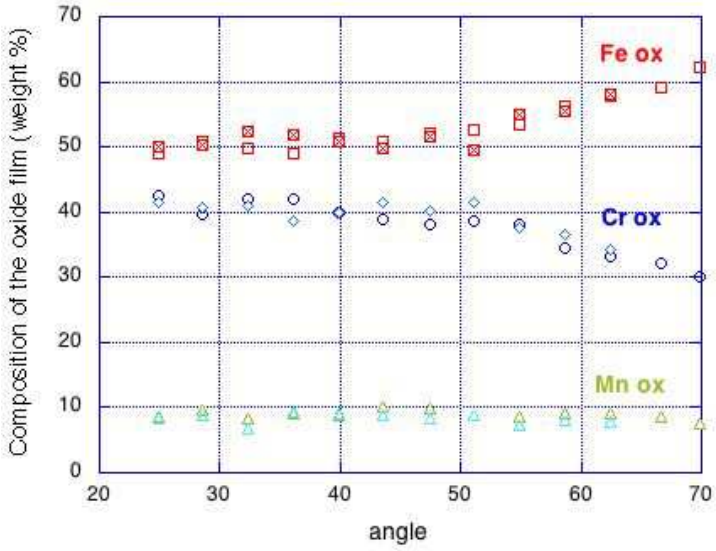

Fig. 3.17 Composition of the oxide film for 1.4456 samples exposed for 1 h to artificial saliva (37°C)

The composition of the passive film for the samples exposed for 1 hour to the artificial saliva is presented in figure 3.17. The composition of the oxide clearly changes at angles higher than 50

degree: the content of oxidized iron increases and that of oxidized chromium decreases, the outer surface of the film has a composition of ca. 60% of iron, 30% of chromium and 10% of manganese; all elements are present in oxidized form. The oxidized manganese content remains constant at ca. 10%. The composition of the alloy beneath the oxide film is given in table 3.9.

Samples exposed for 3 h to the artificial saliva

The composition of the oxide film for the samples exposed for 3 hours to the artificial saliva is presented in figure 3.18. The composition of the oxide changes at angles higher then 45 degree: the content of iron oxide increases and that of chromium oxide decreases, the outer surface of the film has a composition of ca. 60% of oxide, 34% of chromium and about 6% of manganese. The composition of the alloy beneath the oxide film is given in table 3.9.

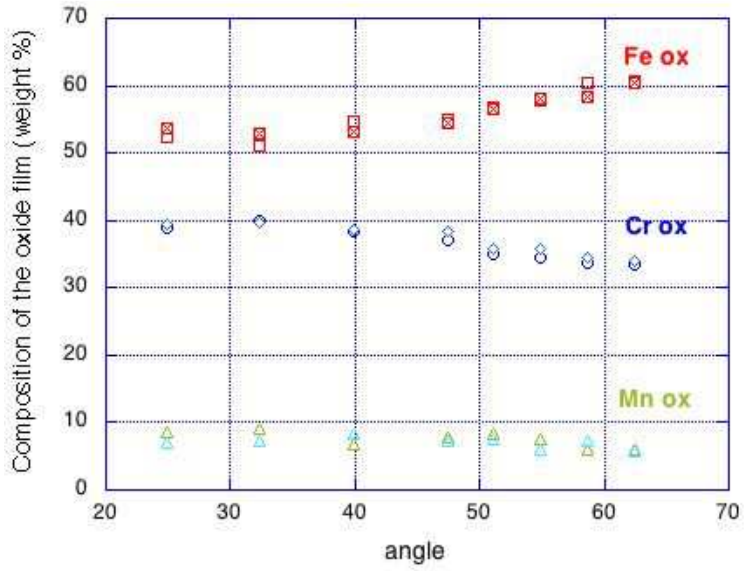

Fig. 3.18 Composition of the oxide film for 1.4456 samples exposed for 3 h to artificial saliva (37°C)

Samples exposed for 16 h to the artificial saliva

The composition of the oxide film for the samples exposed for 16 hours to the artificial saliva is presented in figure 3.19. The composition of the oxide changes at angles higher than 50 degree: the content of oxidized iron increases and that of oxidized chromium decreases, the outer surface of the film has a composition of ca. 60% of iron, 34% of chromium and about 6% of manganese oxy-hydroxides. The composition of the alloy beneath the oxide film is given in table 3.9.

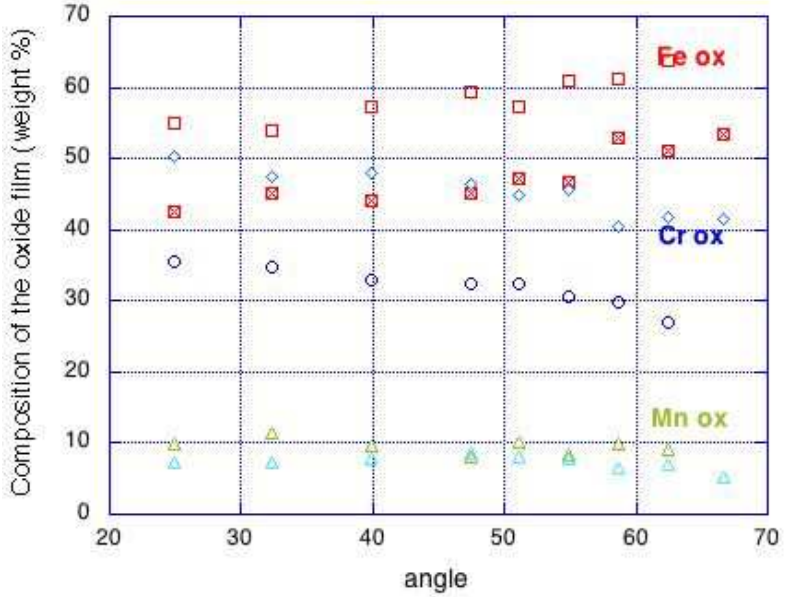

Fig. 3.19 Composition of the oxide film for 1.4456 samples exposed for 16 h to artificial saliva (37°C)

Samples exposed for 24 h to the artificial saliva

The composition of the oxide film for the samples exposed for 24 hours to the artificial saliva is presented in figure 3.20. The composition of the oxide film changes at angles higher than 40 degrees: the content of oxidized iron increases and that of oxidized chromium decreases, the outer surface of the film has a composition of ca. 65% of iron, 25% of chromium and about 8% of manganese. The composition of the alloy beneath the oxide film is given in table 3.9.

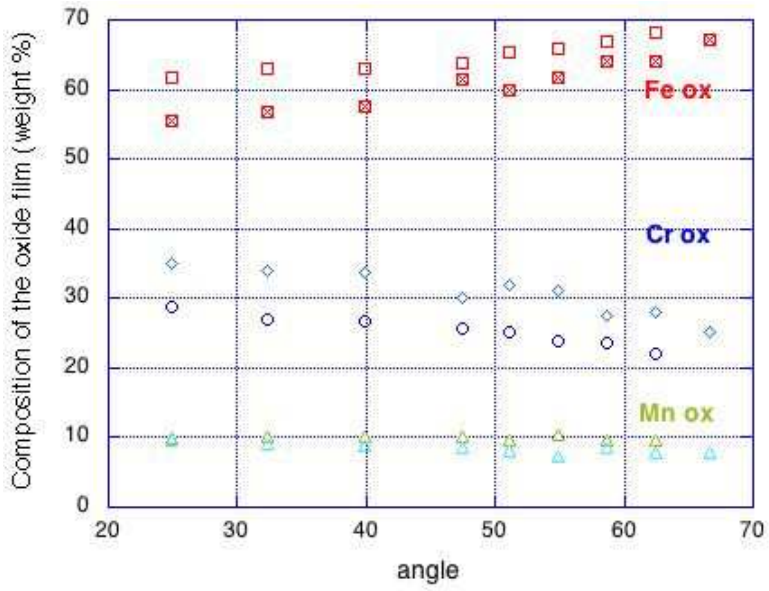

Fig. 3.20 Composition of the oxide film for 1.4456 samples exposed for 24 h to artificial saliva (37°C)

Composition of the alloy interface beneath the oxide film

The three-layer model allows calculating the average composition of the interface beneath the oxide film formed. The thickness of the metal phase that is probed by XPS (sampling depth) diminishes with increasing thickness of the oxide film. Table 3.9 shows the detailed results. An average composition of 70.5 % iron, 16.9% chromium and 12.9% manganese was revealed, indicating that manganese is markedly depleted beneath the oxide film.

Table 3.9: Composition of the alloy beneath the oxide film for 1.4456 samples exposed to artificial saliva (37°C)

Time (h)	sample	Fe mean	Cr mean	Mn mean
1	S1	72.1 ± 3	15.3 ± 2	13.4 ± 2
1	S2	71.9 ± 3	18.1 ± 2	10.3 ± 2
3	S2	69.8 ± 3	16.5 ± 2	13.8 ± 2
3	S3	68.9 ± 3	17.8 ± 2	13.6 ± 2
16	S1	71.6 ± 3	15.6 ± 2	13.2 ± 2
16	S3	68.0 ± 3	17.8 ± 2	14.2 ± 2
24	S2	71.9 ± 3	17.9 ± 2	10.5 ± 2
24	S3	70.2 ± 3	16.1 ± 2	14.1 ± 2
Average		**70.5**	**16.9**	**12**

3.4 Contact angle results

Contact angles were obtained using the sessile drop method with a Krüss contact-angle measuring system (DSA-100, Krüss GmbH, Germany). The drop image was stored by a video camera and the contact angle was calculated from the shape of the drop by an image analysis system. Distilled water drop was placed on each sample surface (8.5 µL/drop) and the corresponding contact angle was measured. Three different regions of the surface were used for each sample and the measured results were averaged. The contact angles results (figure 3.21) show that the increase of the immersion time enhances the hydrophilic character of the passive film with respect to the mechanically polished samples that show a contact angle of 90°. The wettability of the passive film is probably due to a higher content of hydroxides at the outer surface of the passive film.

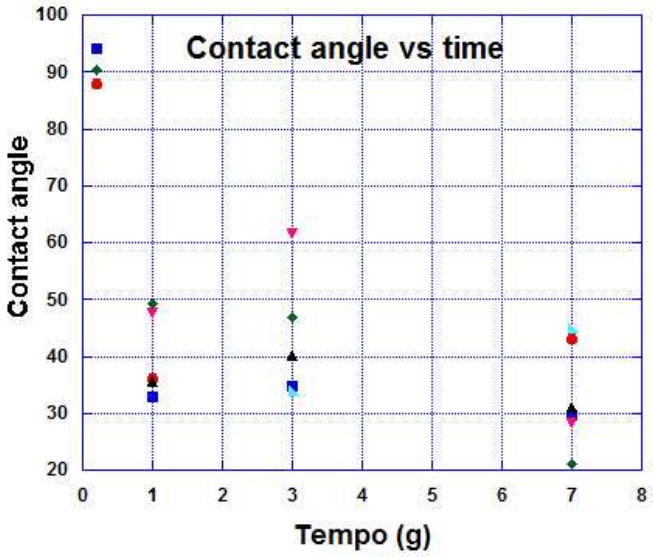

Contact Angle				
	MP	24h	72h	168h
	87.82	32.63	34.43	43.13
	94.01	32.77	34.75	29.75
	90.23	49.15	46.85	21.20
		35.63	40.22	31.50
		47.78	33.88	28.45
				44.77
Average	**90.7±3.1**	**39.6±8.2**	**38.0±5.6**	**33.1±9.1**

Fig. 3.21 Contact angles measured on DIN 1.4456 samples exposed for to artificial saliva (25°C)

3.5 Results of ICP analysis

The solutions from the microcells (each ca. 0.5 ml) were conserved and later analysed for their chemical composition with ICP. The solution (or sometimes dry residues) was dissolved in 1 mL of artificial saliva. 500 µL of each resulting solution was diluted to 25 mL with HNO_3 2% (w/w) in ultrapure water.

Table 3.10 Results of the ICP measurements

Exposure	Iron µg/L	Chromium µg/L	Manganese µg/L
7d	0.6 (0.3)	0.14 (0.09)	nd
7d	0.28 (0.06)	0.18 (0.07)	nd
7d	0.71 (0.08)	nd	nd
7d	0.4 (0.1)	nd	0.14 (0.07)
7d	0.22 (0.05)	nd	nd
3d	0.3 (0.1)	nd	nd
3d	0.44 (0.07)	nd	nd

The ICP results (table 3.10) show very low amount of metal release from the DIN 1.4456 stainless steel samples to the artificial saliva. It has however to be considered that all these values (each sample three independent ICP measurements) are below the detection limit for the metal ions analysed. Only the release rate of iron can be considered meaningful. It can be observed that the release rates are not very different between exposure time 3 or 7 days indicating that the main dissolution occurs at the beginning of the exposure.

References

[1] A.Rossi, B. Elsener, *Materials and Corrosion*, 63, N°12, 2012

[2] B. Elsener, D. Addari, S. Coray, A. Rossi, *Electrochimica Acta*, Volume 56, Issue 12, 30 April 2011, 4489-4497

[3] D. Addari, B. Elsener, A. Rossi, *Electrochimica Acta,* Volume 53, Issue 27, 2008, 8078–8086

[4] A. Rossi and B. Elsener, *Surface and Interface Analysis*, 18 (1992) 499 – 504

4 Discussion

4.1 General

In this chapter the electrochemical results (OCP, linear polarization) and the XPS surface analytical results will be discussed regarding the corrosion resistance and thus biocompatibility of orthodontic brackets made of the nickel-free DIN 1.4456 stainless steel. Literature results and previous work [1] performed in our laboratory will be included for comparison and to complete the picture, especially regarding the comparison between exposure at 25°C and at 37°C. On the basis of all results a model for the dissolution and passivation of the alloy in artificial saliva is proposed.

4.2 Corrosion resistance of the Ni-free stainless steel DIN 1.4456

Dental alloy materials should have good mechanical properties and a high corrosion resistance in order to not release potentially toxic metal ions (to be biocompatible). Despite the oral cavity is a potentially highly corrosive environment the materials used for dental alloys have to show only negligible corrosion rates. In order to get meaningful results in a short period electrochemical methods are frequently used. In this work open circuit potential and linear polarization measurements were used. For a series of experiments the solution was analysed by ICCP.

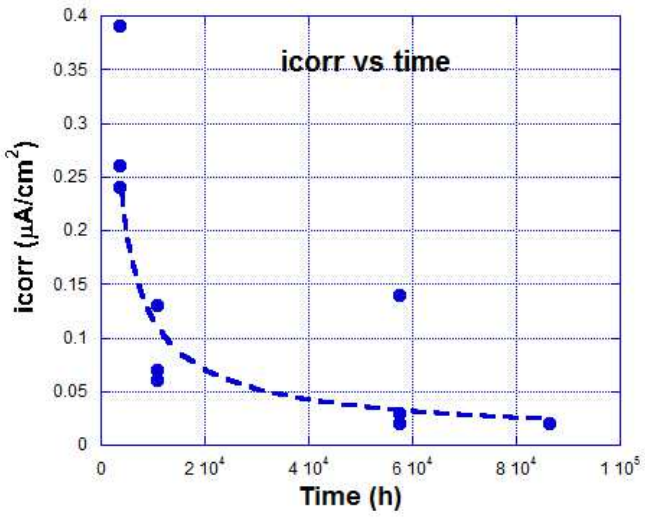

Figure 4.1 Corrosion current density versus time for DIN 1.4456 immersed in artificial saliva 37°C

From the linear polarization resistance measurements (chapter 3.2.2) the corrosion current density i_{corr} was calculated (see table 3.1 and 3.2). The plot of corrosion current density versus time shows that the dissolution rate of the alloy is markedly decreasing over time as is expected

for an alloy that is forming a protective passive film. Passivation is further confirmed by the anodic polarization curve (figure 3.9) with a dynamic corrosion current density of ca. 2 µA/cm^2, much higher compared to the steady state value of < 0.02 µA/cm^2. Other research papers from literature [2,3,4] indicate a value of the corrosion rate of about 2.5*10^{-6} (A/cm^2).

From the values of the corrosion current density the corrosion rate in µm/year has been calculated (table 3.1, 3.2). Integration of the corrosion rate over time leads to the total weight loss during the exposure time. For 3 days result 2.47 µg, for 7 days 3.10 µg. These values are estimates and determined to a great extent by the initially high corrosion rate. The solutions from the micro-cell experiments (open circuit potential see figures 3.5 and 3.6) were later analysed by ICP analysis. The results (chapter 3.5) show that the concentrations of iron, chromium and manganese detected were very low (iron 0.2 to 0.7 µg/L) thus indicating that essentially the nickel-free stainless steel DIN 1.4456 is in the passive state in artificial saliva. The initially high corrosion current densities (figure 4.1) lead to a rapid transformation of the surface film into a protective passive film.

4.3 Surface state of the Ni-free stainless steel DIN 1.4456

In this work two series of experiments have been performed: one using the conventional electrochemical cell with exposure times up to 24 h and operating at 37°C (chapter 3.3.3), the other with micro-cells with exposure times up to 7 days but operating at 25°C (chapter 3.3.2). First the two series will be discussed separately, in a following paragraph they will be compared.

4.3.1 Experiments at 37°C

Mechanically polished samples have been exposed to solutions of artificial saliva using the electrochemical cell with about 200 ml of solution (chapter 2.2.3). Open circuit potentials were measured for 1 to 24 h exposure. At the end of the exposure time the polarization resistance was measured (chapter 2.2.3). After removing from the cell the sample was washed, dried and then analysed by angle-resolved XPS (chapter 2.3.2). For each exposure time two samples (replica) were studied. The results of the angle-resolved XPS analysis are presented in detail in chapter 3.3.3.

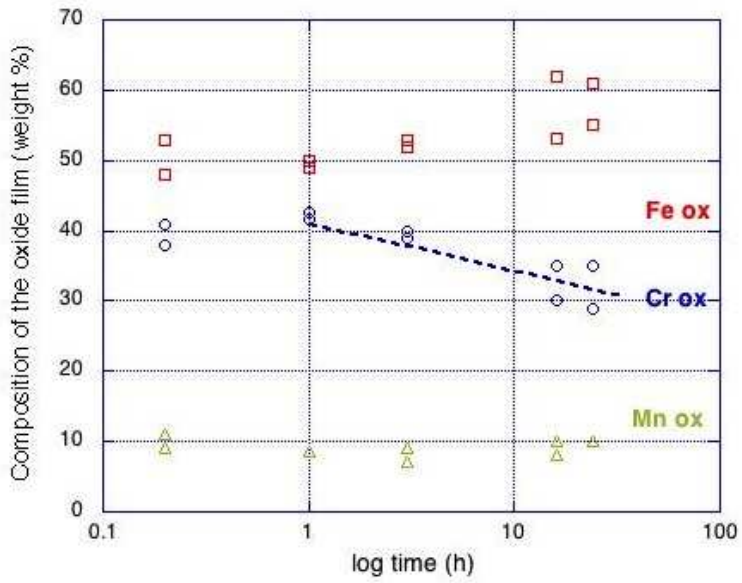

Figure 4.2 Cation composition of the oxy-hydroxide film formed on DIN 1.4456 immersed in artificial saliva 37°C for exposure time up to 24 hours. Average over emission angles 24.8 to 48 degree.

Condensing the results allows studying the influence of exposure time both on the composition of the oxy-hydroxide film that formed during exposure and on the alloy beneath the film. Figure 4.2 shows the cation composition of the oxide film. It can be observed that the oxy-hydroxide film changes its composition with exposure time. The content of oxidized iron increases from 50 to 60%, oxidized chromium decreases from 40% to 30% and oxidized manganese remains constant at

10%. Molybdenum signals were not recorded due to the poor signal to noise ratio in ARXPS measurements. Note that at the outer part of the film iron content was found to be even higher and chromium content slightly lower.

The alloy composition beneath the film has been calculated for all measurements with the three-layer model [5]. As is shown in figure 4.3 the alloy composition beneath the film remains remarkably constant at 68 ± 1% iron, 14.9 ± 1.3 % manganese and 16.9 ± 1% chromium. The average composition at angles from 55 to 66 degree in ARXPS is slightly different, 73.5 ± 1.3 iron, 10.1 ± 1.1 manganese and 16.0 ± 1.3% chromium. These values indicate a concentration gradient beneath the oxide film with a marked depletion of manganese immediately beneath the oxy-hydroxide film.

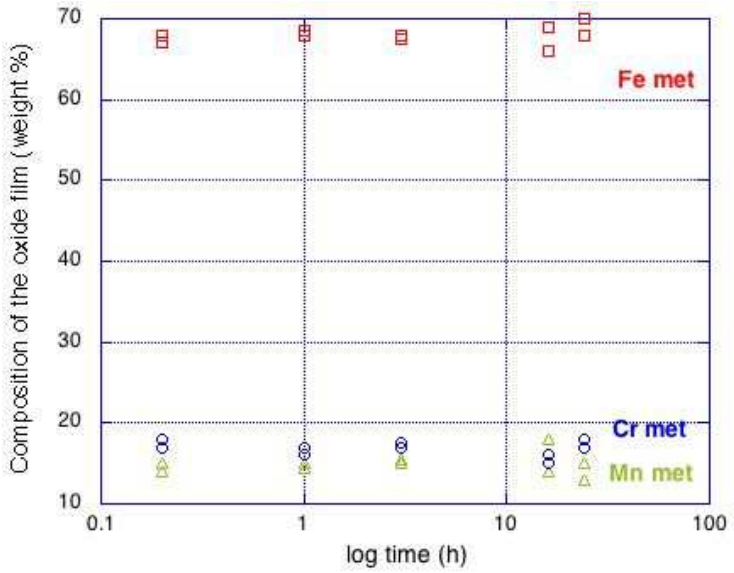

Figure 4.3 Composition of the alloy beneath the oxy-hydroxide film formed on DIN 1.4456 immersed in artificial saliva 37°C for exposure time up to 24 hours. Average over angles 24.8 to 48 degree.

4.3.2 Experiments at 25°C

Mechanically polished samples have been exposed to solutions of artificial saliva using the micro-cells (chapter 2.2.3). A small amount of solution was permanently in contact with the sample surface. At the end of the exposure period the samples were washed and analysed by XPS (chapter 2.3.2). For each exposure time three samples (replica) were studied. The results of the XPS analysis are presented in detail in chapter 3.3.2.

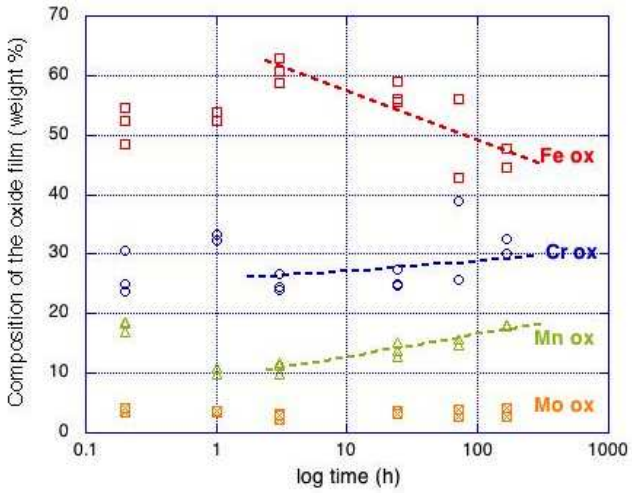

Figure 4.4 Cation composition of the oxy-hydroxide film formed on DIN 1.4456 immersed in artificial saliva 25°C for exposure time up to 7 days

Condensing the results allows studying the influence of exposure time both on the composition of the oxy-hydroxide film that formed during exposure and on the alloy beneath the film. Figure 4.4 shows the cation composition of the oxide film. It can be observed that the oxy-hydroxide film changes its composition with exposure time. At three hours of exposure the film has about 60% of oxidized iron, 25% oxidized chromium, 10% of oxidized manganese and 5% of oxidized molybdenum. Longer exposure times lead to a decrease in oxidized iron, an increase in oxidized manganese to 20% and a slight increase in oxidized chromium.

After 30 sec of sputter cleaning with Argon ions an XPS measurement was performed again (see table 3.6). The contamination layer and most of the oxy-hydroxide film was removed, the composition of the residual oxide film is shown in figure 4.5 It can be noted that great part of the iron oxide has been removed; the residual oxide film is composed of about 35% of manganese oxide, 30% chromium oxide, 30% iron oxide and 7% molybdenum oxide. No clear trend with exposure time con be noted except a slight decrease of the manganese oxide content.

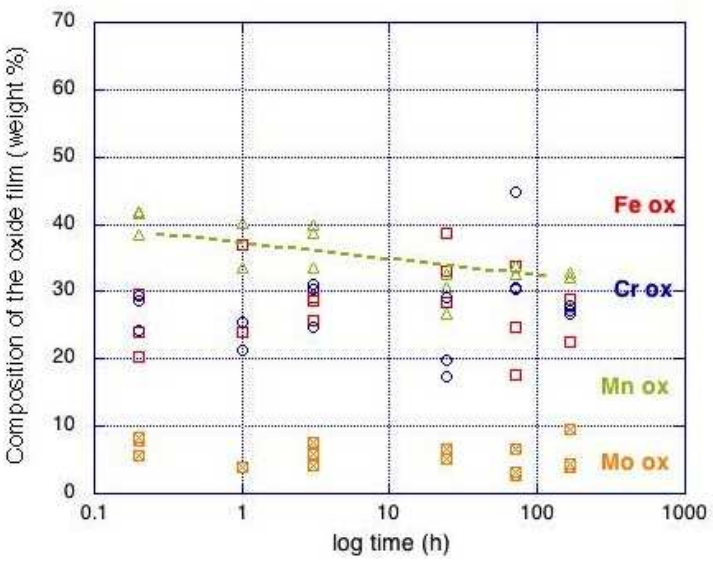

Figure 4.5 Cation composition of the oxide film after 30 sec of sputtering. DIN 1.4456 immersed in artificial saliva 25°C for exposure time up to 7 days

The composition of the alloy immediately beneath the oxy-hydroxide film (table 3.5) greatly differs from the bulk alloy as has been reported for other stainless steels in neutral [6] and alkaline media [7,8]. The results show that the chromium and molybdenum content approximately correspond to the bulk composition whereas the manganese is markedly depleted (between 4 and 9 weight %). The composition seems to be reasonably constant over the different exposure times.

The composition of the alloy beneath the oxide film does not change significantly when determined after 30 sec of sputtering (table 3.7). Chromium is found with 18.2 ± 1%, molybdenum with 4.3 ± 0.4 % and iron with 71.1 ± 1.9%. The concentration of manganese in the alloy beneath the film varies with the residual oxide film thickness (figure 3.13). This might be explained by a concentration profile of manganese beneath the oxide film: immediately beneath the oxide film manganese is strongly depleted (ca. 5%), at greater depth the bulk concentration will be reached. This point is further discussed in paragraph 4.5.

After 300 sec of sputtering a steady state composition is reached (table 3.8). In table 4.1, the average steady state composition is compared with the bulk composition of the alloy. It can be noted that the iron content corresponds to the bulk composition whereas molybdenum is strongly enriched, chromium slightly enriched and manganese strongly depleted. This might be explained by preferential sputtering where heavy elements (molybdenum) become enriched and lighter elements with a lower melting point (manganese) are removed easier.

Table 4.1 Comparison of the steady state composition reached after 300 sec of sputtering and the bulk composition of the alloy DIN 1.4456

Condition	Fe	Mn	Cr	Mo
300 sec of sputtering	59.3 ± 0.7	11.6 ± 0.3	22.3 ± 0.5	6.7 ± 0.3
bulk	60.1	18.4	17.9	1.9

4.4 Comparison between 25°C and 37°C

Experiments regarding the corrosion resistance of the nickel-free stainless steel DIN 1.4456 have been performed at 25°C and at 37°C, covering thus room temperature and body temperature. For practical applications one has to consider that the temperature in the oral cavity can vary between 5°C and 55 °C.

The open circuit potentials at both temperatures show an asymptotic increase with time of exposure to the artificial saliva (figure 4.6). Despite some scatter in the open circuit potentials it clearly can be seen that the final potentials (24 h) are more positive at 37°C. Long term experiments in the micro-cells performed at 25°C showed open circuit potentials of ca. -80 mV SCE after 7 days of immersion (chapter 3.2.1).

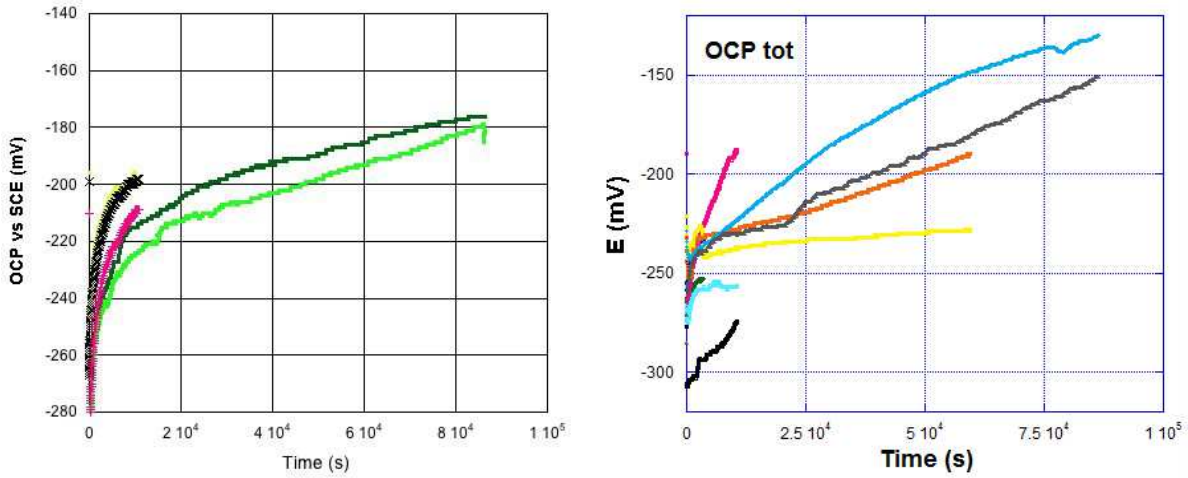

Figure 4.6 Evolution of the open circuit potential with time for DIN 1.4456 immersed in artificial saliva at 25°C (left) [1] and 37°C (right).

Table 4.2 Average Rp and vcorr values of the alloy DIN 1.4456 immersed in artificial saliva at 25°C [1] and 37°C

Time	Rp 25°C	Rp 37°C	vcorr 25°C	vcorr 37°C
h	MΩ* cm2		µm/year	
1	0.29	0.18	1.81	3.45
3	0.52	0.68	1.3	1.01
16	0.68	1.42	0.82	0.74
24	1.15	2.67	0.50	0.23

The average values of the measured linear polarization resistance Rp at 37°C (chapter 3.2.2) and at 25°C [1] as well as of the corrosion rate calculated are compared in table 4.2. From the graphical

representation where all single values are included (figure 4.7) it can be noted that the corrosion rate at short times is higher at 37°C, at longer exposure times the situation is reversed.

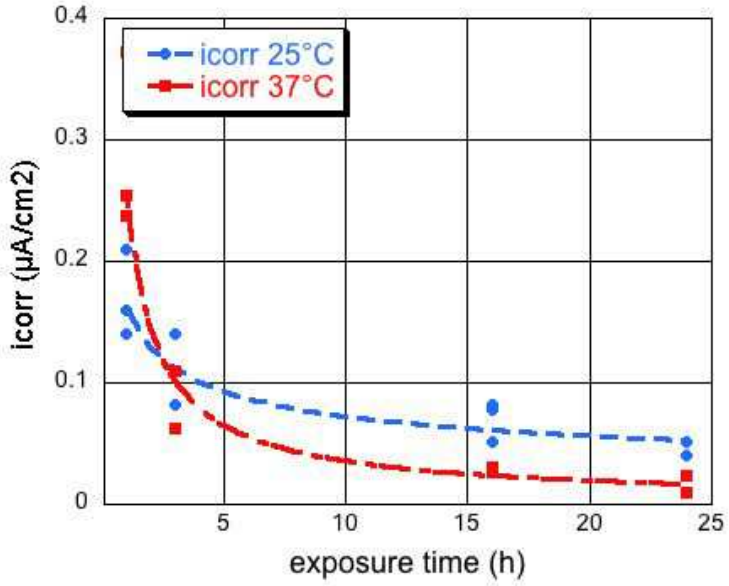

Figure 4.7 Corrosion rate versus time of the alloy DIN 1.4456 immersed in artificial saliva at 25°C [1] and 37°C

In order to get some more information on the kinetics, the data are plotted in a log vcorr vs log time diagram, where a straight line indicates a power law. As can be noted from figure 4.8 the slope at 25°C is lower then at 37°C indicating that the decrease in corrosion rate are faster at 37°C. Thus negligible corrosion rates should be reached faster at higher temperatures.

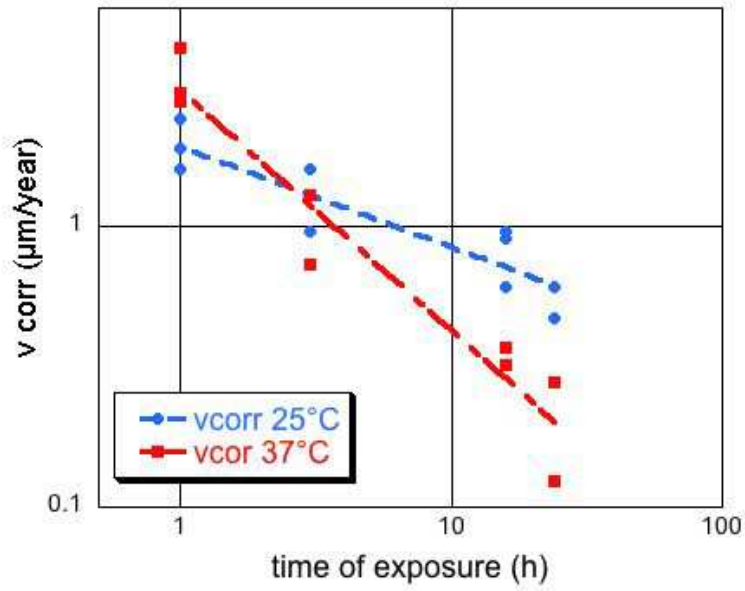

Figure 4.8 Corrosion rate versus time (log-log plot) of the alloy DIN 1.4456 immersed in artificial saliva at 25°C and 37°C

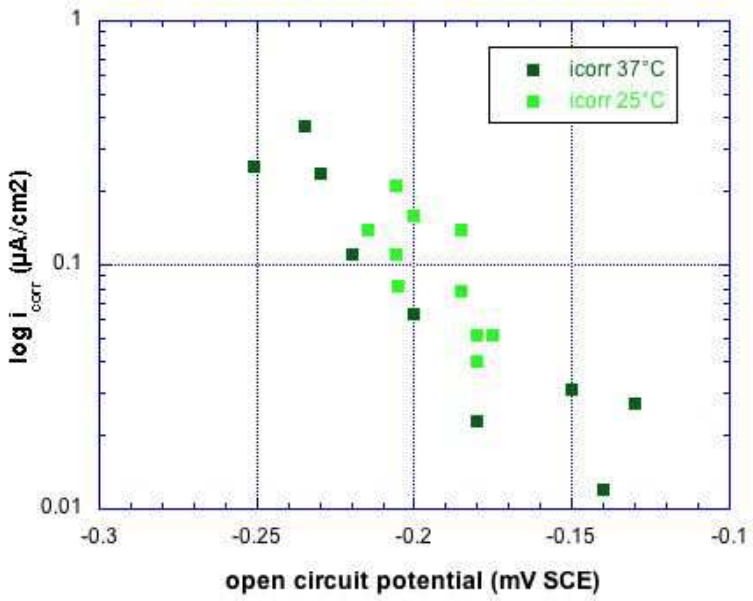

Figure 4.9 log Corrosion current density icorr versus open circuit potential. Measurements from the alloy DIN 1.4456 immersed in artificial saliva at 25°C and 37°C for different times

The corrosion current density i_{corr} for a given corrosion system is related to the open circuit potential. For the measurements at 25°C [1] and at 37°C this is shown in figure 4.9. As can be noted the values obtained at the two temperatures fall with reasonable accuracy on the same trend line (negative slope of ca. – 60 mV/decade) indicating that the same electrochemical reactions (cathodic tafel slope) are involved.

4.5 Model for the dissolution / passivation of the DIN 1.4456 alloy

When immersing stainless steel specimens having the surfaces covered by mechanically polished- or air formed oxide films, the compositions of the latter will change until a steady state (stable passive film) has been reached. The following assumption for this surface film transformation on stainless steels in artificial saliva solutions is outlined for the manganese-bearing DIN 1.4456 stainless steel with 18% of manganese and 18% of chromium (figure 4.10a): *Iron* dissolves preferentially and becomes depleted at the film/bulk interface and is present in the passive film mainly as Fe(III) oxi□hydroxide, its total content in the film decreaseas with more positive *ocp*'s (i.e. increasing immersion time). *Chromium* is preferentially oxidised and accumulates in the passive film as Cr (III) oxi-hydroxide whereas at the interface it reaches the bulk composition after prolonged immersion (table 3.9). The less noble *manganese* dissolves like iron and is depleted at the film/bulk interface. *Molybdenum* oxy-hydroxides are slightly enriched in the passive film (figure 4.4). Owing to the decrease of manganese the interface becomes enriched in *iron* (figure 4.3).

Note, as discussed in chapter 4.2, the dissolution of the alloy occurs mainly in the first few hours, later only iron is released at a low rate. Thus at longer exposure times mainly film transformation occurs.

DIN 1.4456 **DIN 1.4301**

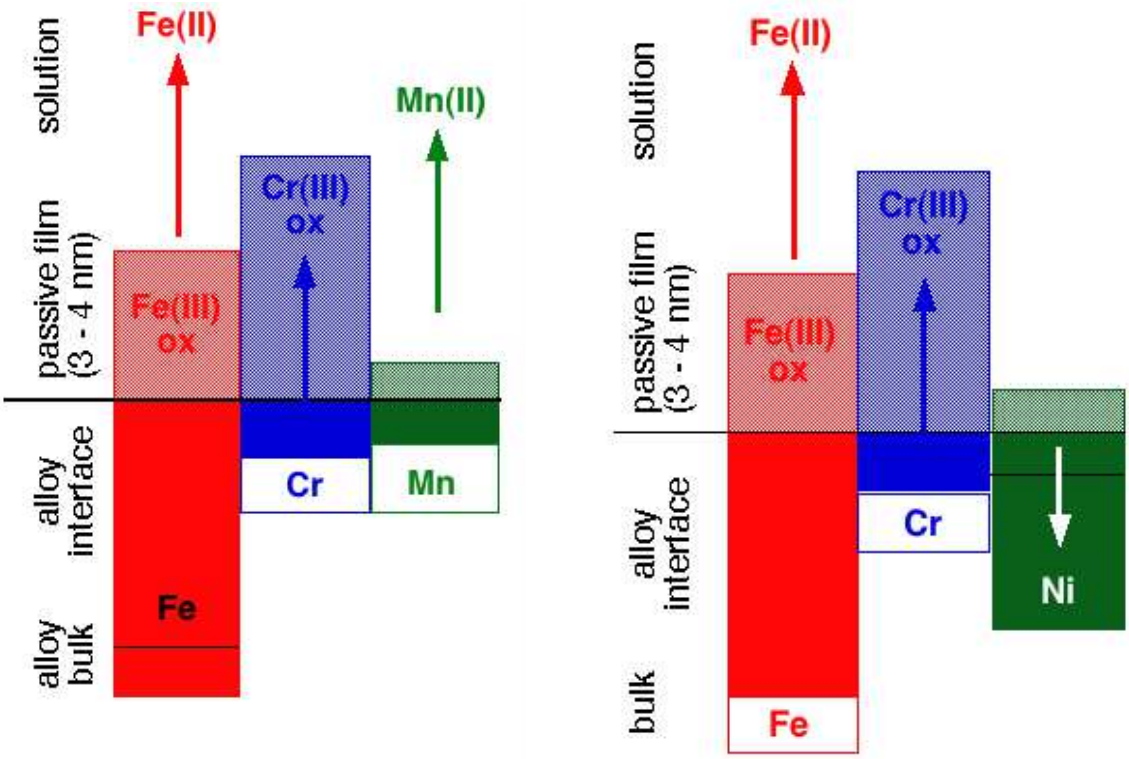

In contrast to the nickel-free DIN 1.4456 stainless steel, the conventional DIN 1.4301 stainless steel with 8% nickel shows a strong enrichment of nickel (the most noble alloy component) immediately below the oxy-hydroxide film [9] (at the interface).

References

[1] M. Mazza, Indagine elettrochimica sulla biocompatibilità di un acciaio al manganese in saliva artificiale. Tesi di laurea, Università degli Studi di Cagliari, 2010

[2] M. Pakshir, T.Bagheri, M.R. Kazemi, European Journal of Orthodontics, 2011

[3] N.J.E. Dowling, Y.-H. Kim, S.-K. Ahm, Y.-D. Lee, Corrosion Engineering Section, 1999, Vol. 55, No.2

[4] N. Schiff, F.Dalard, M. Lissac, L. Morgan, B. Grosgogeat, European Journal of Orthodontics 27 (2005) 541-549

[5]A. Rossi and B. Elsener, Surface and Interface Analysis, 18 (1992) 499 – 504

[6] A. Rossi, R. Tulifero and B. Elsener, Materials and Corrosion 52 (2001), 175-180

[7]D. Addari, B. Elsener, A. Rossi, Electrochemistry and surface chemistry of stainless steels in alkaline media simulating concrete pore solutions, Electrochimica Acta 53 (2008) 8078-8086

[8] D. Addari, Nanosized films on the surface of stainless steels. PhD Thesis, Università degli studi di Cagliari, 2005

[9] A. Rossi, B. Elsener, Materials and Corrosion, 2012,63, N°12

5 Summary and conclusion

In this PhD thesis the stability of the Ni-free stainless steel DIN 1.4456 in artificial saliva has been studied with electrochemical and XPS surface analytical techniques at 25°C and at 37°C with respect to its use as dental or orthodontic alloy. The results have shown that the alloy forms a protective passive film at both temperatures. The kinetics of initial dissolution and film formation are more rapid at 37°C compared to 25°C but seem to follow the same mechanism. At 37°C the initial corrosion rate is much higher but its decrease with time is more rapid. After 24 h the dissolution rate is already lower then 0.2 µm/year, the steady state dissolution rate will be at least one decade lower. This very low dissolution rate has been confirmed by solution analysis by ICP where the metal ion concentration was found to be below the detection limit of the technique for all the alloy elements.

A great effort has been undertaken to characterize the composition of the surface film formed after different times of exposure. At 25°C the oxy-hydroxide film formed is enriched in oxidized chromium, after long immersion times (7 days) the nominal composition of oxidized manganese (18%) is found. Molybdenum in the film is slightly enriched. Angular resolved XPS performed on samples exposed at 37°C clearly indicate that the outer part of the passive film is composed essentially of iron oxy-hydroxide whereas chromium oxy-hydroxide is located at the inner part. From experiments with argon ion sputtering it results that the inner part of the film is enriched in oxidized chromium and manganese, oxidized iron is strongly depleted. The alloy beneath the passive film results to be depleted in manganese both from angle-resolved XPS and from experiments with sputtering.

Finally a model is proposed that might explain the surface films formed after exposure to artificial saliva solution. During the short initial period with a relatively high corrosion rate iron and especially manganese (non-noble elements) dissolve. Chromium is the film-forming element and an inner chromium oxy-hydroxide film is formed. This film limits progressively the dissolution of the alloy: with time an outer iron oxy-hydroxide film is formed. Due to the dissolution of manganese the manganese content immediately below the film is strongly depleted. On the contrary, molybdenum is present with about 7%. Such a layered structure of the surface is responsible for the high corrosion resistance and biocompatibility of the DIN 1.4456 stainless steel.

Acknowledgements

I wish to express my warmest thanks to:

Prof. Antonella Rossi for giving the opportunity to work on an interesting research project and for her introduction to surface analysis, encouragement and advice.

Prof. Bernhard Elsener for the thorough introduction into the electrochemical methods and their interpretation. The motivating discussion with him and critical way to address scientific problems were an important factor in improving the quality of my work.

Dr. Danilo Addari for his scientific and personal support, especially in the first year of the Ph.D. work and for the numerous scientific discussions.

Dr. Marzia Fantauzzi for being a pleasant office-mate and for the useful and interesting discussions about x-ray photoelectron spectroscopy.

Prof. Nicholas D. Spencer for giving me the possibility to spend a period of three months at the Swiss Federal Institute of Technology Zurich during which I had not only a fruitful scientific experience but also the possibility to meet new friends.

Mr. Clément Cremmel for his valuable support during the contact angle measurements.

Mr. Giovanni Cossu for his technical help during the XPS measurements with the Quantera.

Dr. Francesco Caruso and Sara Mantellato of the Institute Building Materials, Corrosion and Durability for their help with the AES-ICP measurements.

I would also like to thank all the former members of the group of Surface Analysis, Electrochemistry and Corrosion at the Università degli Studi di Cagliari and the Colleagues I met during my stay at the LSST in Zurich.

Manuela Pisu gratefully acknowledges Sardinia Regional Government for the financial support of her PhD scholarship (P.O.R. Sardegna F.S.E. Operational Programme of the Autonomous Region of Sardinia, European Social Fund 2007-2013 - Axis IV Human Resources, Objective l.3, Line of Activity l.3.1.)".

Appendix I

Calibration of the AlKα source Theta Probe with associated errors

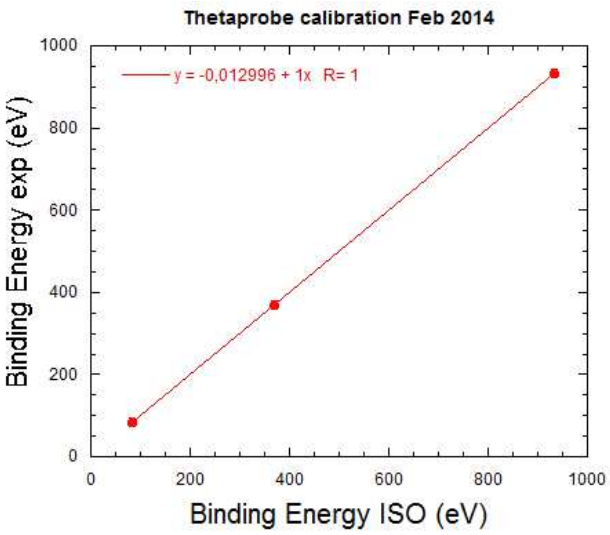

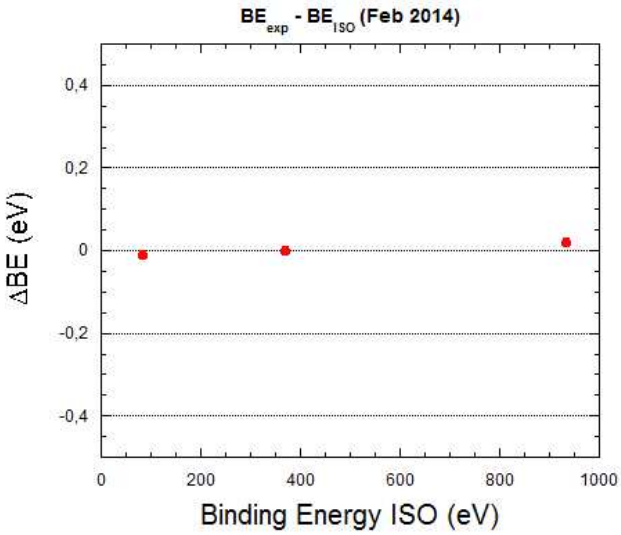

Appendix II

Composition profile after 300 sec. of ion argon sputtering at temperature of 25°C of the sample DIN 1.4456 for all time immersion and mechanically polished. Have been reported only one profile for each time immersion.

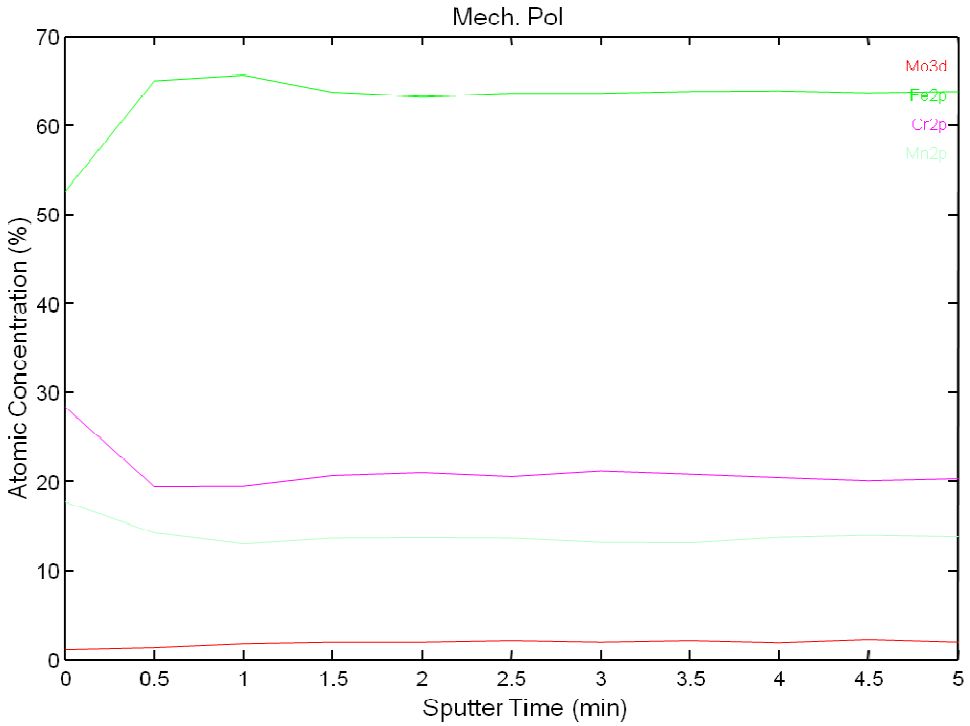

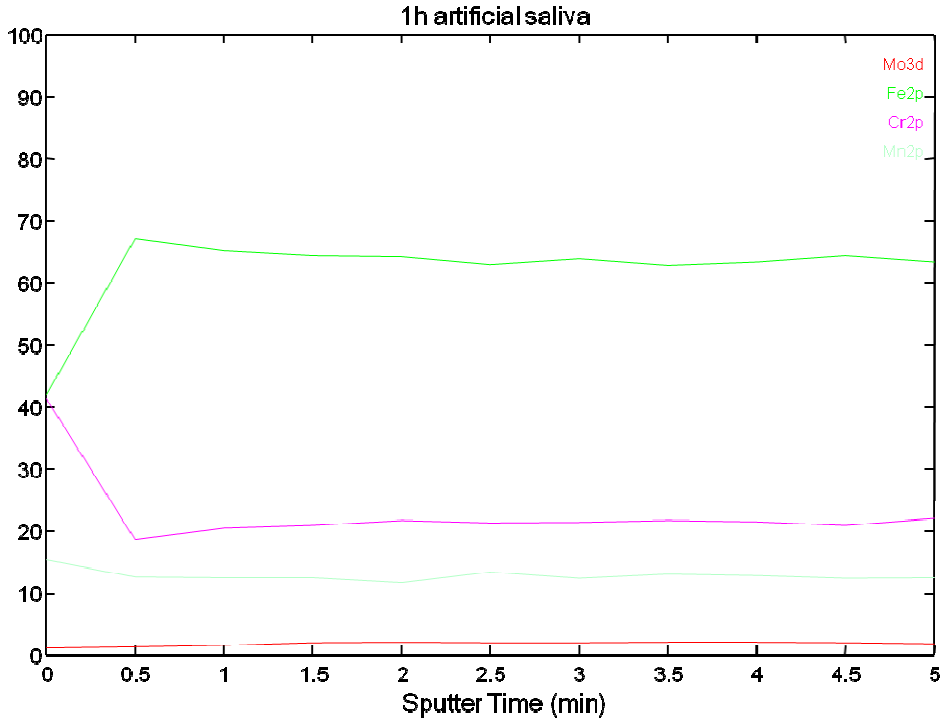

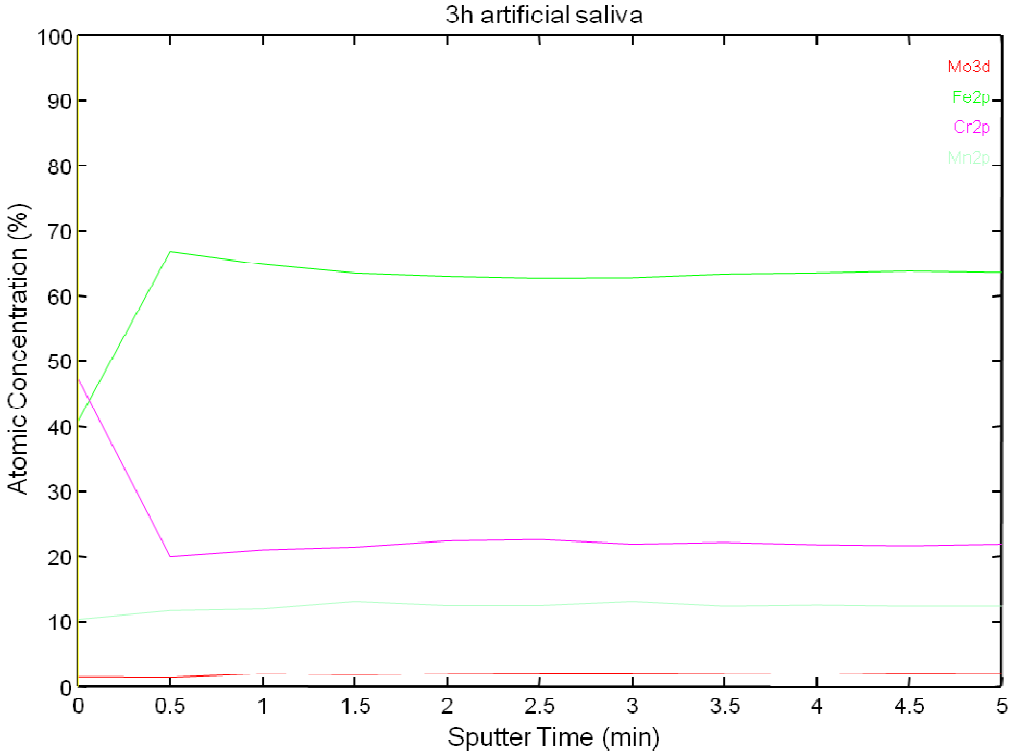
3h artificial saliva
Mo3d
Fe2p
Cr2p
Mn2p
Atomic Concentration (%)
Sputter Time (min)
0
10
20
30
40
50
60
70
80
90
100
0
0.5
1
1.5
2
2.5
3
3.5
4
4.5
5

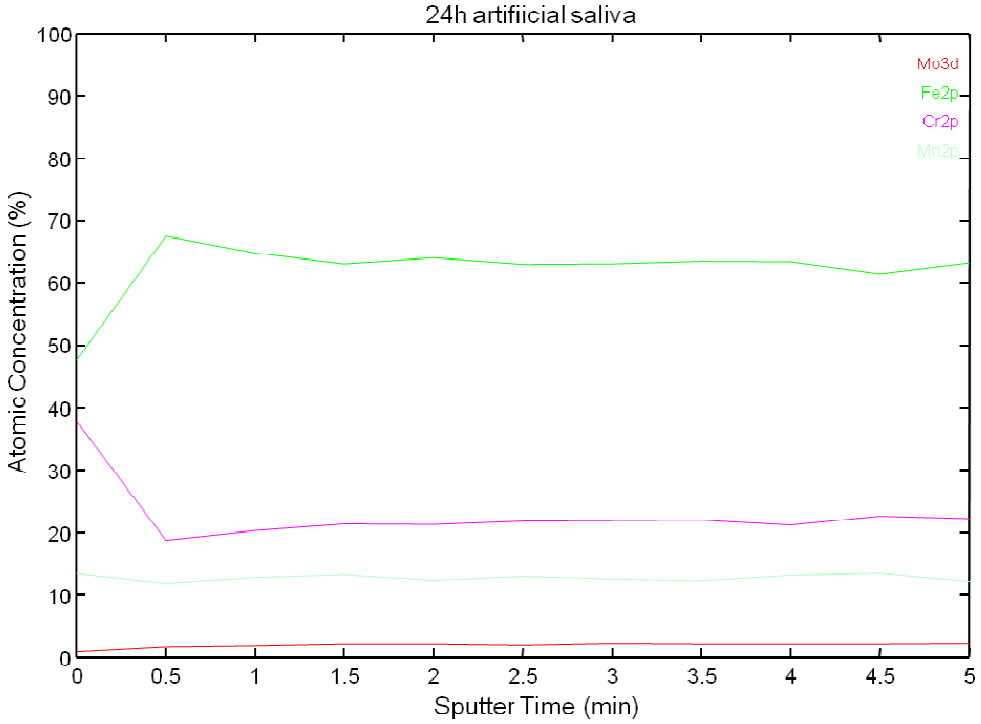
24h artifiicial saliva
Mo3d
Fe2p
Cr2p
Mn2p
Atomic Concentration (%)
Sputter Time (min)
0
10
20
30
40
50
60
70
80
90
100
0
0.5
1
1.5
2
2.5
3
3.5
4
4.5
5

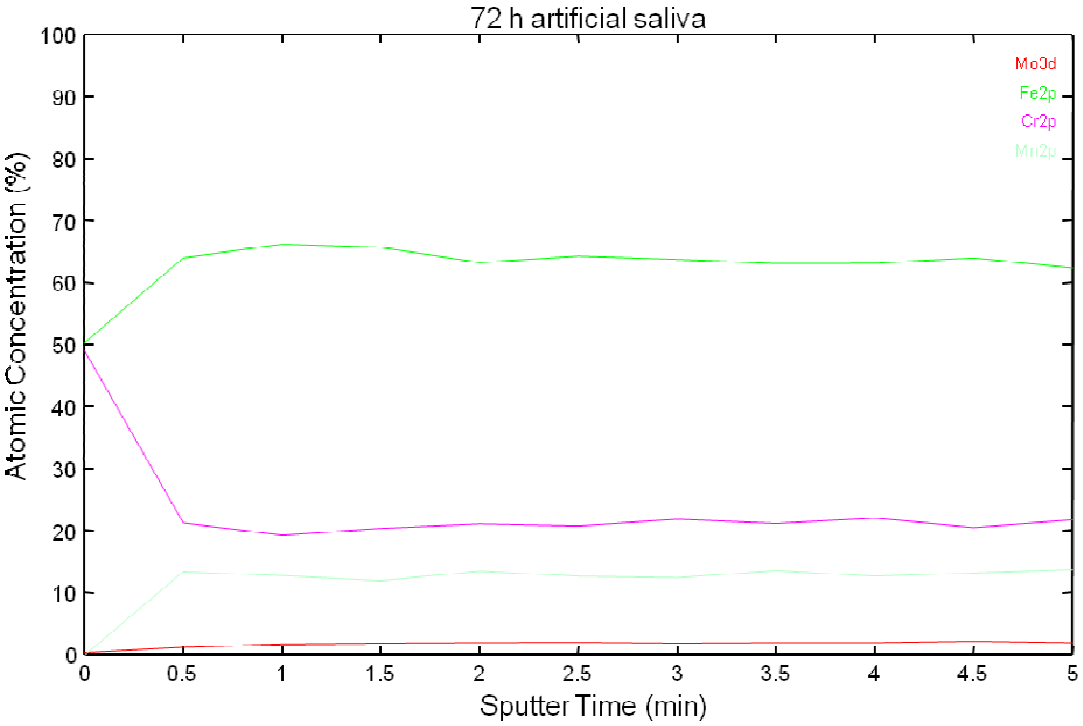
72 h artificial saliva
Mo3d
Fe2p
Cr2p
Mn2p
Atomic Concentration (%)
Sputter Time (min)
0
10
20
30
40
50
60
70
80
90
100
0
0.5
1
1.5
2
2.5
3
3.5
4
4.5
5

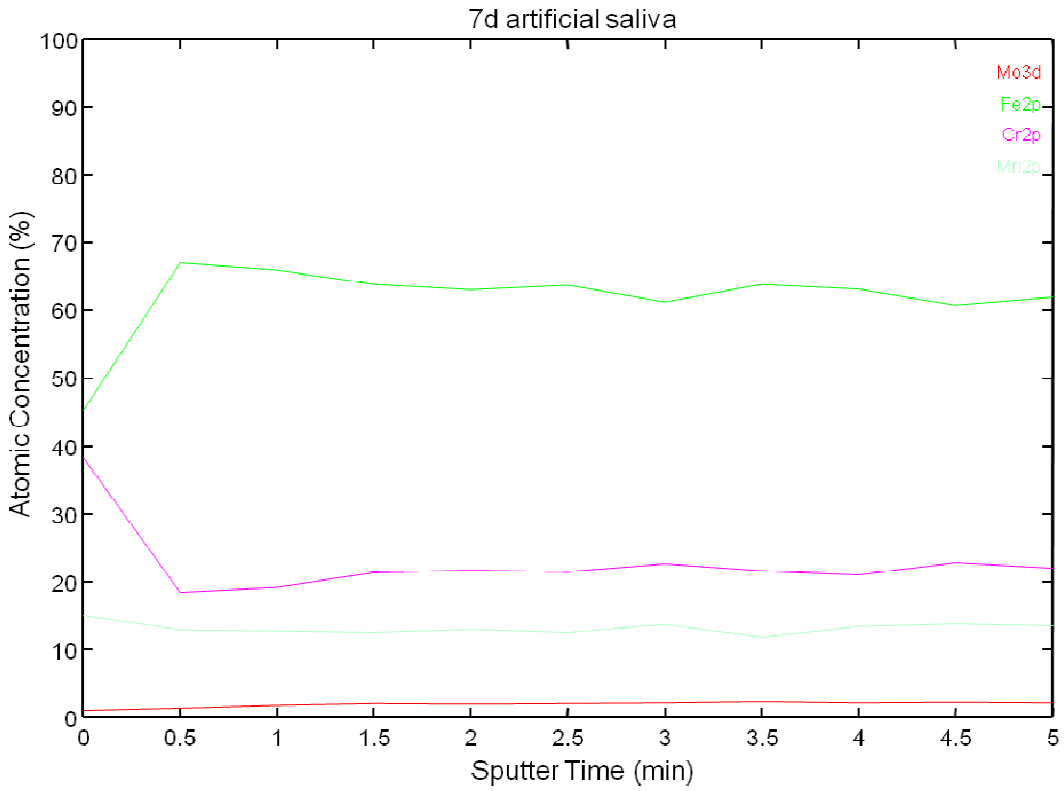
7d artificial saliva
Mo3d
Fe2p
Cr2p
Mn2p
Atomic Concentration (%)
Sputter Time (min)
0
10
20
30
40
50
60
70
80
90
100
0
0.5
1
1.5
2
2.5
3
3.5
4
4.5
5

Appendix III

Peak fitting parameters-PHI Quantera SXM spectrometer

Signal	Component	Pos. constrain	Line shape
Fe 2p 3/2	Fe (0)	706.9-706.7	GL(85)T(0.80)
	Fe (II) oxide + sat.	709.7-709.3	GL(30)
	Fe (III) ox	711.2-710.8	GL(30)
	Fe ox-hy	712.4-712	GL(30)
Cr 2p 3/2	Cr (0)	574.1-573.9	GL(65)T(1)
	Cr (III) oxide	576.6-576.4	GL(30)
	Cr (III) hy	578.1-577.9	GL(30)
Mn 2p 3/2	Mn (0)	638.9-638.6	GL(80)T(1)
	MnO	641.238-640.838	GL(90)
	MnO_2	642.9-642.5	GL(90)

Peak fitting parameters-Theta Probe spectrometer

Signal	Component	Binding Energy (eV)	G/L
$Fe2p_{3/2}$	Fe (0)	706.8 ± 0.1	GL(85)T(0.80
	Fe (II) oxide + FeO sat.	709.4 ± 0.1 714.8 ± 0.1	GL(30)
	Fe (III) oxide	710.8 ± 0.1	GL(30)
	Fe oxy-hydroxide	712.4 ± 0.1	GL(30)
$Cr2p_{3/2}$	Cr(0)	573.9 ± 0.1	GL(65)T(1)
	Cr(III) oxide	576.4 ± 0.1	GL(30)
	Cr (III) hydroxide	577.9 ± 0.1	GL(30)
$Mn2p_{3/2}$	Mn (0)	638.9 ± 0.1	GL(80)T(0.55)
	MnO	641.2 ± 0.1	GL(90)
	MnO_2	642.5 ± 0.1	GL(90)

Appendix IV

Spectra after sputtering of Chromium , Iron, Manganese, Molybdenum